Final Report for DOE/EERE Project 7543

Project Title:	Device Architecture for Next Generation CdTe PV
Project Period:	08/01/2016 – 07/31/2020
Submission Date:	10/19/2020
Recipient:	Colorado State University
Address:	Department of Physics Fort Collins, CO 80525-1875
Award Number:	DE-EE0007543
Project Team:	Colorado State University National Renewable Energy Laboratory
Principal Investigator:	James Sites, Professor Phone: 970-491-5850 Email: james.sites@colostate.edu
Business Contact:	Lisa Anaya, Senior Research Administrator Phone: 970-491-0537 Email: lisa.anaya@colostate.edu
Acknowledgment:	“This material is based upon work supported by the Department of Energy, Office of Energy Efficiency and Renewable Energy (EERE), under Award Number DE-EE0007543.”
Disclaimer:	

Executive Summary

The overall project objective has been to enhance the device architecture of CdTe solar cells in ways that contribute to their performance without compromise of cost-effective manufacturability. The project contributors included James Sites, Jennifer Drayton, Alexandra Bothwell, Tao Song, Andrew Moore, Anna Wojtowicz, Pascal Jundt, Ramesh Pandey, and Darius Kuciauskas (NREL). The primary technical milestones focused on higher cell voltage and efficiency, and the significant contributions to the CdTe device structure, with full references in body of report, are as follows:

● Thin CdTe Absorbers. Two objectives for thinner CdTe cells were to have fully depleted absorbers to enhance the effectiveness of electron reflection at the back interface and to show that thinner cells with lower materials cost and production time were viable. In comparison to thicker cells with standard 3-µm CdTe, the thin ones also had well-behaved current-voltage characteristics, no reduction in voltage, and very respectable efficiencies: 15% with 1.0-µm CdTe and over 10% with 0.4 µm [Bothwell, Drayton, and Sites, IEEE J. Photovoltaics 10, 259 (2020)].

● Te Layer to Enhance the Back Contact. A tellurium layer with a valence-band energy intermediate between the CdTe absorber and Ni used for the back contact was added between the two to replace the CdTe/metal barrier to holes with two smaller ones. This configuration, which is particularly important for the thinner cells, increased cell efficiency and allowed voltage above 1 volt at reduced temperatures [Song, Moore, and Sites, IEEE J. Photovoltaics 8, 293 (2018)].

● Bilayer CdSeTe/Te Cells. The thin-absorber approach was extended with a bilayer of a CdSeTe alloy in front of CdTe, a strategy developed by GE and First Solar. Replacing the first 0.5 µm of CdTe with the lower band-gap CdSeTe produced cells with 2 mA/cm^2 higher current, only a partial reduction in voltage, and a much larger photoluminescence response consistent with voltage being closer to its ideal value [Bothwell, Drayton, Jundt, and Sites, MRS Advances 4, 37 (2019)].

● CdMgTe Layer for Electron Reflection. The purpose was to reflect electrons from the rear of the cell with a layer of CdMgTe, an alloy with the band gap expanded primarily in the conduction-band direction, to direct electrons towards the front for higher current and to reduce the hole barrier. This structure was partially successful; current and voltage were increased, but the voltage did not achieve the project milestone [manuscript led by Bothwell in preparation].

● Front-Interface MgZnO Buffer. MgZnO had earlier replaced CdS at Colorado State because its higher band gap transmits shorter-wavelength photons and it has a favorable conduction-band offset with CdTe. Other labs, however, have had mixed results. The reason appears to be been low electron density, partially mitigated in some cases by photogeneration, but now seen to be better addressed by doping the MgZnO with Ga [Pandy, Shimpi, Munshi, and Sites, IEEE J. Photovoltaics, in press].

In addition to the specific cell results, there were two important development projects: The first was professional visual publication of the process for fabricating the cells [Bothwell, Drayton, Jundt, and Sites, J. Visualized Experiments 157 (2020)]. The

second was a broader interpretation of time-resolved photoluminescence (TRPL) data by varying the voltage bias across a completed cell. In sufficient forward bias, the diode field is eliminated and the lifetime of the absorber can be reliably measured [manuscript led by Jundtin preparation].

During the course of the project, the research team maintained close contact the industrial CdTe community, especially First Solar, Inc., and with CdTe researchers at several other universities and at NREL. The results summarized above now appear in the published literature as noted above and have been presented at several conferences and workshops. Of the six students involved in the project, three (Song, Moore, and Bothwell) completed their Ph.D., and one (Wojtowicz) her thesis M.S. The other two (Jundt and Pandey) should complete the Ph.D. in 2021.

Table of Contents

Background

Prior to the start of this project, CdTe panels manufactured by First Solar, had achieved a substantial share of the photovoltaic market in the U.S., particularly for utility scale installations. By 2016, the First-Solar company had in addition to its solid performance achieved long-term reliability [1] and excellent life-cycle health and safety [2], as well as short energy-payback time and low carbon footprint [3]. During the past four years the volume of CdTe PV production has continued to increase, reaching to 5.4 GW at First Solar in 2019 [4], helped in large part by the introduction of its Series 6 panels. Today, about one third of U.S. PV power comes from CdTe panels. At the same time, smaller companies including Toledo Solar in the U.S., CTF solar based in Germany, and Advanced Solar Power in China have been bringing additional CdTe factories on line. The understanding of CdTe PV at the cell level has also continued to expand through a variety of investigation at several different institutions. A major focus has been the the use of group-V dopants such as As to increase the carrier density of the CdTe absorber [5]. This period has also seen an increased level of communication and collaborative research among the institutions within the CdTe community.

Introduction

The project plan (SOPO) has had four parts corresponding to the four project years. In each case, there was a fabrication task focused on one or two layers of the cell and a characterization, analysis, and simulation task on the cell as a whole. Figure 1 shows the layers of the completed cell with the numbers beside key layers indicating which layer received the primary attention in each of the four project years. The layers are deposited from the glass upwards; in operation light would enter from the glass side. During the project there were approximately 100 deposition runs of 6-8 substrates each and 10-25 cells on each substrate. These runs included several variations on the cell structure shown and not all the layers were used for each set of cells.

The first year of the project focused on thin CdTe (1a), and it achieved good efficiencies for CdTe absorbers much thinner than 1 µm. It also focused on the Te layer at the back of the cell (1b), which was particularly important for the thin-absorber cells. The second year, following the lead of First Solar and GE, added the CdSeTe alloy layer (2), which allowed higher current densities. The third project year added the CdMgTe layer at the back of the cell for electron reflection (3). This task carried over into the fourth year (4), where advances in different parts of the cell,

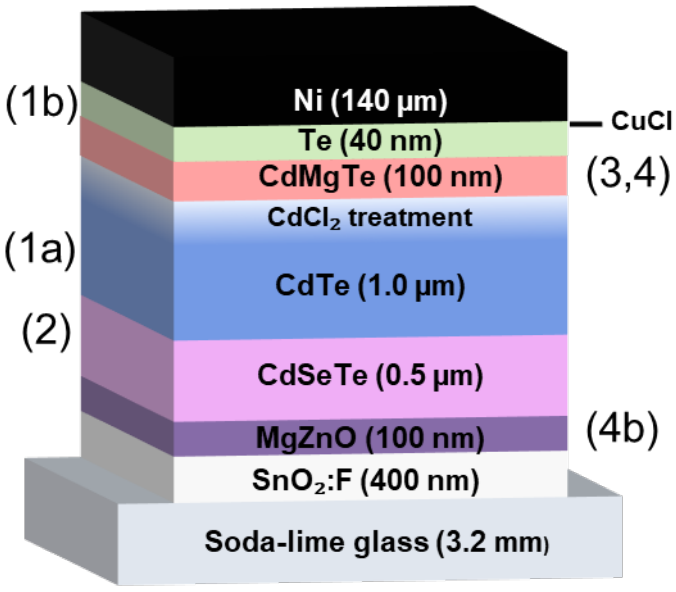

Figure 1. Cell structure with focus area for each of 4 years noted.

including better understanding of the MgZnO buffer layer at the front of the cell (4b), were integrated.

Throughout the four years of the project, a large number of cells were fabricated and key performance parameters and materials properties such as elemental profiles were carefully measured. Cell understanding was advanced through integration of these measurements with quantitative analysis and device simulations. In the course of the work, improvements were made to the fabrication facilities [6] and to the analytical techniques employed. Particularly helpful has been the addition of voltage-bias dependence to the interpretation of spectral and time-resolved photoluminescence measurements.

Project Results and Discussion

Thin CdTe Absorbers. The primary purpose of thin CdTe has been to create a fully depleted absorber to be used in conjunction with a back surface field to allow photocurrent collection at higher voltages, and hence increase the open-circuit voltage of the cell. An additional purpose from a manufacturing standpoint is the use of less CdTe material and the reduction in processing time. This work in Year 1 was primarily performed by PhD student Alexandra Bothwell, MS student Anna Wojtowicz, and research associate Jennifer Drayton. The results appear in Ref. [7].

Previous studies showed that CdTe cells with polycrystalline absorbers of 1 µm or less and CdS emitters that were fabricated by magnetron sputtering [8-10], metalorganic chemical-vapor transport [11], and vapor-transport deposition [12] were able to yield cells with respectable efficiencies. The thin cells in this study, shown in Fig. 1 and similar to thicker ones in our lab, had a polycrystalline CdTe absorber, which was deposited by close-space sublimation (CSS) onto the MgZnO buffer layer, and completed with a $CdCl_2$ passivation step, Cu-doping at the back, and a Te layer that will be discussed in the following section.

Figure 2 shows a dark-field scanning transmission electron microscope (STEM) image a cell with a 1-µm CdTe absorber. The CdTe grains extended throughout the thickness of the absorber, and although the layers at the small thickness are rough, the MgZnO layer below and Te layer above the CdTe are conformal, and there is no indication of void formation.

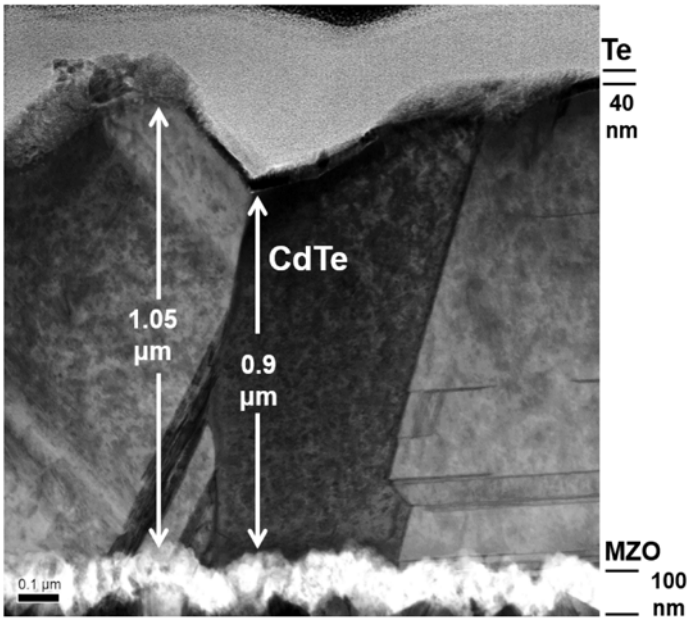

Figure 2. Cross-section image of thin CdTe cell.

Current-voltage curves from a series of cells with CdTe thicknesses between 0.4 and 1.2 μm are shown at the left in Fig. 3, and the device parameters from the five highest-efficiency cells in each case are shown to the right. The 1.2-μm efficiency reached 15% with V_{OC} of 847 mV, J_{SC} of 24.0 mA/cm^2, and fill-factor of 74.0%. The 1.0-μm cells had very similar parameters, and the thinner ones showed systematic reductions in current and fill-factor, but only minimal decreases in voltage.

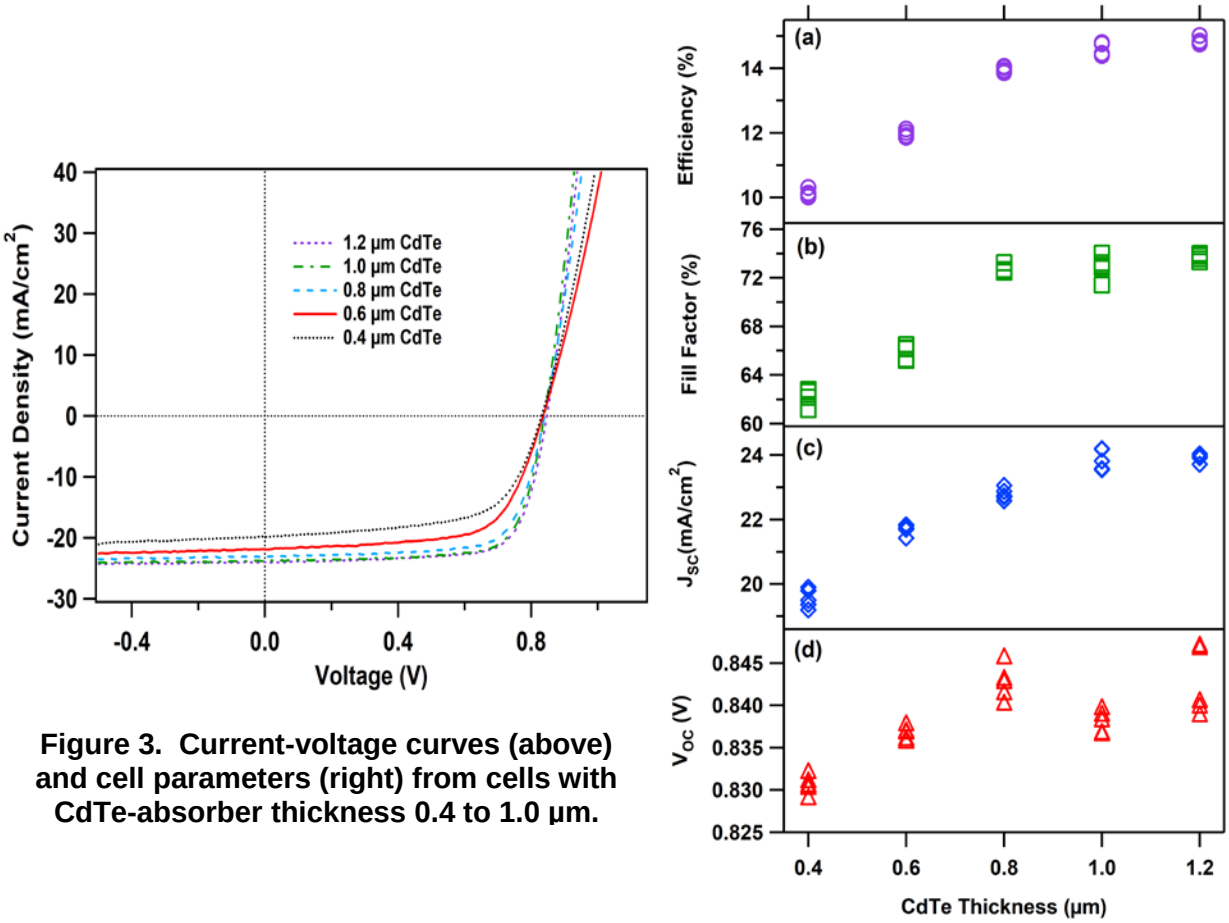

Figure 3. Current-voltage curves (above) and cell parameters (right) from cells with CdTe-absorber thickness 0.4 to 1.0 μm.

Capacitance measurements from the sets of cells in Fig. 3 were consistent with the physical thicknesses of the cells and showed that the thinner ones were fully depleted. The carrier density appeared to be near 10^{15} cm^{-3} for most of the cells, but was difficult to evaluate for the thinnest ones.

To evaluate the decline in fill-factor for the thinner absorbers, the series resistance R_S, shunt conductance G, and diode quality factor A were extracted from the J-V curves. Although each contributed the fill-factor reduction, the largest impact at the smaller thicknesses came from an increase in diode quality factor from 1.6 at 1.2 μm to above 2 at the smaller ones.

The individual current losses, which were the largest change with the thinner cells, are shown for the 0.4 and 1.2-μm cells in Fig. 4. The current loss from the fall-off in quantum efficiency near the band gap, labeled incomplete absorption, is what is expected from the absorption spectrum of CdTe. The separation of photon losses was

done with optical measurements following each deposition step. Reflection is shown in black, glass absorption in darker green, TCO absorption in lighter green primarily at short wavelengths, negligible MZO absorption, and remaining loss assumed to be from electron-hole recombination before collection.

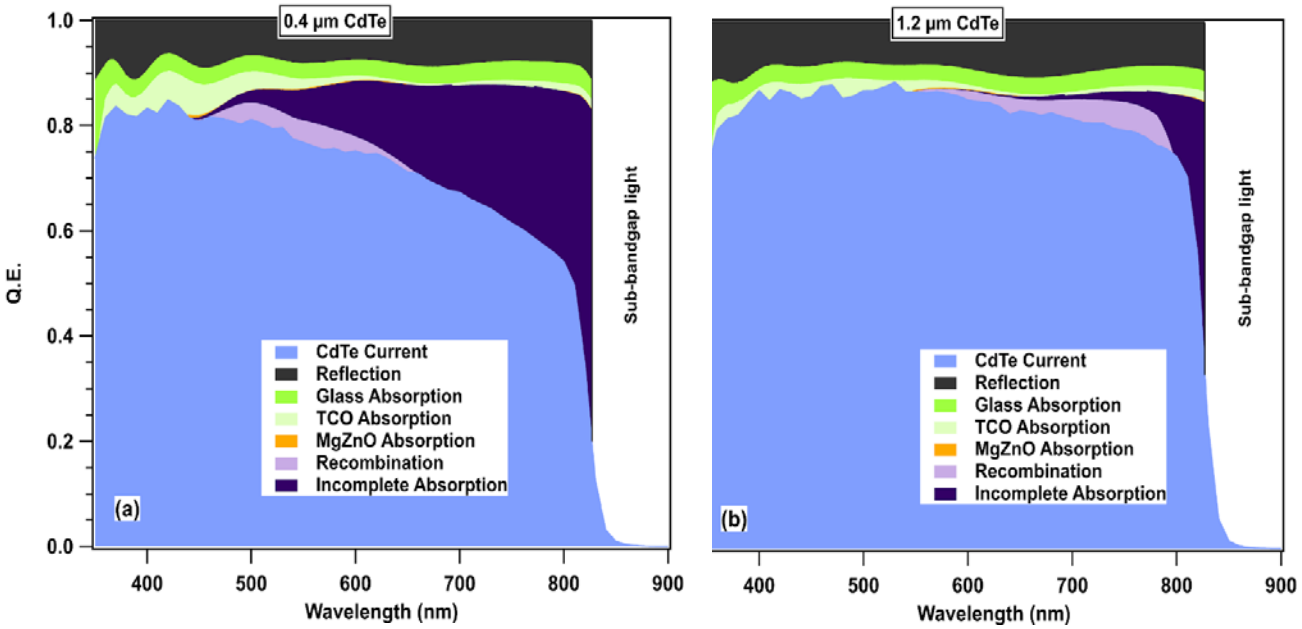

Figure 4. Quantum efficiency and individual photon losses in thinnest and thickest cells.

Further insight on the effect of thin absorbers is found in spectral luminescence (PL) and time-resolved photoluminescence (TRPL). The spectral PL in Fig. 5 shows that the primary peak is close to the CdTe band gap in all cases. The PL intensity, however, is significantly larger for the thicker cells, and it roughly scales with thickness. Since the front layers of all cells was nominally the same for all absorber thicknesses, this suggests that recombination at the back interface of the CdTe is the dominant factor revealed by the spectral PL.

The TRPL measurements tracked the decay of the PL signal following a short excitation pulse. They were performed at NREL on cell structures where the metal contact behind the Te layer was omitted so that light could enter from either side of the

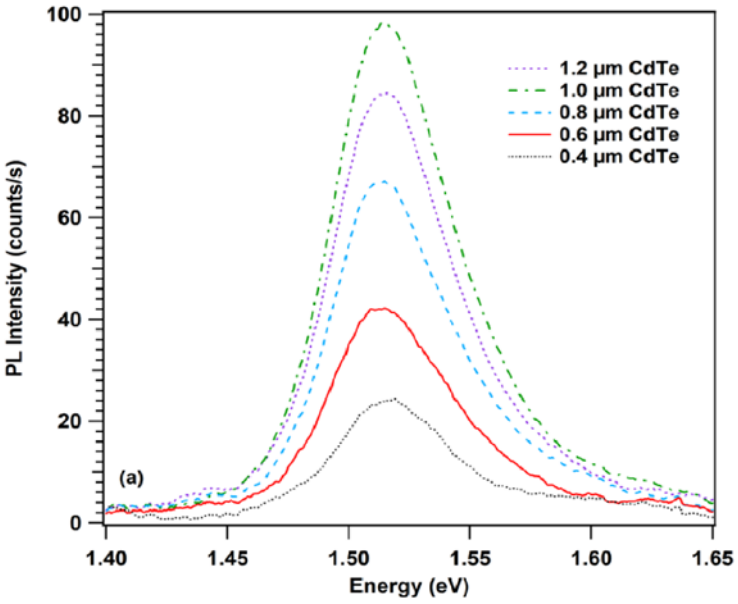

Figure 5. PL spectra from cells of different thickness.

cell. The penetration depth of the excitation beam was ~0.2 µm, so there was a clear difference in the region probed between front and rear entry for all but the thinnest cells.

TRPL decay curves for excitation from the glass (front) and Te (back) sides of the cells with CdTe thickness ranging from 0.4 to 2.0 µm are shown in Fig. 6. The front-side decay times increase significantly for the larger thickness, whereas the back-side times are in a narrow range similar to the front-side values for the thinnest cells. The front-side values extrapolate to approximately 6 ns, which should be a good estimate of the bulk recombination lifetime for the CdTe layers. The back-side values remain near 0.5 ns, a lifetime that corresponds to a back interface recombination velocity slightly below 10^5 cm/s, which is high enough to significantly limit the voltage.

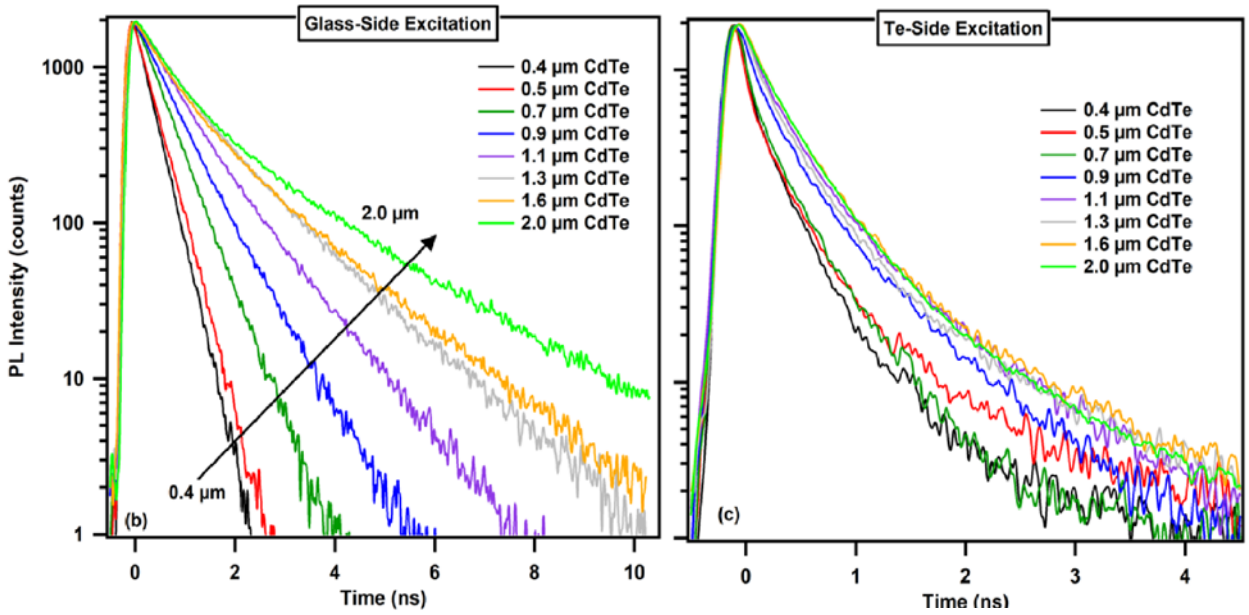

Figure 6. TRPL decay curves for front and back excitation for several CdTe absorber thicknesses.

The primary takeaway from the thin-absorber work is that very thin CdTe absorbers are viable. Going forward, 1 µm of CdTe was taken as the baseline thickness for both CdTe-only cells and the CdSeTe/CdTe bilayer absorbers discussed in a later section.

Te Layer to Enhance Back Contact. The purpose of a thin tellurium layer between the CdTe absorber and the metallic back contact, a second part of the Year 1 task, was to help mitigate the band bending that occurs at the back interface and at the same time reduce the amount of copper-doping needed for a good electrical contact. It was particularly helpful with the thinner absorbers where the back contact is closer to the primary diode junction. Experimental work and corresponding simulations on the impact of the Te layer was done by PhD students Tao Song and Andrew Moore. This work was published in Ref. [13] which built on earlier work [14] by the same students.

Contacting p-type CdTe without distorting the current-voltage curves and compromising cell performance has been a long-term challenge. Previous experimental studies [15-

18] had shown that the Te layer added to the back contact can improve cell performance, but there had been only limited analysis of the mechanism. The current-voltage curves shown in Fig. 7 compare cells made with and without the tellurium layer, and there is a clear interplay with the amount of copper used.

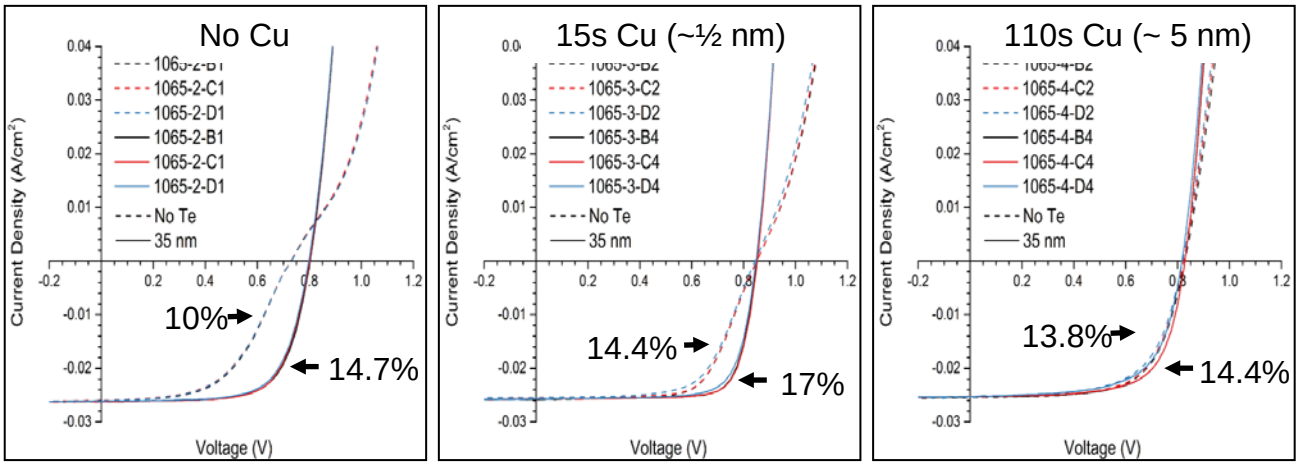

Figure 7. Current-voltage curves for cells with and without the Te layer for different amounts of Cu-doping.

The rightmost panel in Fig.7 shows J-V for several cells made with and without the Te layer when a relatively large amount of Cu-doping was used with the contact. The Cu-doping, shown in Fig. 1, was achieved by depositing a thick CuCl layer, followed by an annealing step, which was estimated to yield approximately 5 nm of copper. All of the cells were completed with the standard Ni external contact. With the heavy dose of copper, the tellurium makes a negligible difference, because the Cu-doping itself forms a good contact. The cells' fill-factor and efficiency, however, is reduced because the copper also diffuses throughout the CdTe, and the resulting defect states lower the recombination lifetime of the CdTe.

At the other extreme as shown in the left panel, the dashed curve is for a cell with neither Cu nor Te. It has a serious distortion, and it has low voltage and efficiency. In this case the Te layer is clearly helpful, but it only yields a mid-level efficiency. The center panel for a small amount of copper, little more than an atomic layer, shows that without the Te layer, the distortion is less, and the efficiency was improved. With the combination of the small amount of copper and the Te layer, very respectable efficiencies were achieved. The Te layer was found by Hall measurements to have a relatively high hole concentration in the mid-10^{18} cm^{-3} range. This would correspond to full depletion for thicknesses below about 30 nm, which were seen to produce lower voltages. The baseline Te thickness was therefore selected to be 40 nm, and the baseline Cu deposition time going forward was 15 s in the middle panel.

The optimization of the Cu/Te combination is also clearly shown in J-V measurements as a function of temperature. Figure 8(a) has no Te in the contact; the carbon (C) in this case was simply used to give a conformal covering before the larger-grain Ni. Figure 8(b) is for an otherwise identical cell that does have the Te layer. These two cells did

have the now standard Cu-doping and would be the two cells in the middle panel of Fig. 8. Without the Te layer in 8(a), the voltage and fill factor are slightly lower than with the Te in 8(b). As temperature is reduced, however, the differences become much larger.

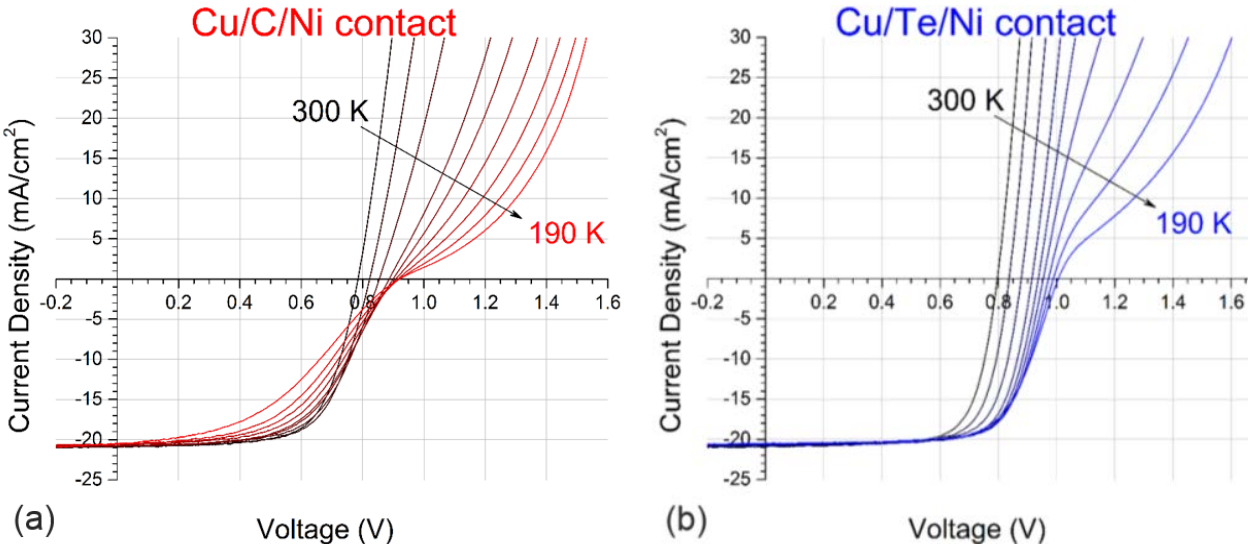

Figure 8. J-V curves as a function of temperature for cells with (a) and without (b) Te as part of the back contact.

The difference between 8(a) and (b) is clear evidence of reduction in the hole barrier at the back contact when the Te layer is present. Without the Te, the kink in the J-V curve becomes much larger and the increase in open-circuit voltage at the lower voltages saturates. With the Te layer, however, the development of the kink and the saturation of V_{OC} occur at significantly lower temperatures.

The differences in the dependence of V_{OC} on temperature are in quite large as can also be seen in Fig. 9. V_{OC} for the cells without the Cu-doping saturates at about 800 or 920 mV depending on whether the Te layer is used. With the high Cu-doping, the saturation voltage is higher, but with the more optimal Cu-doping and the Te layer, the voltage does not saturate within the temperature range available (down to 175 K), and a CdTe cell voltage of 1.07 V is seen in Fig. 9. The key point for the cell structure is that the barrier to hole collection at the rear of the cell is substantially reduced with the Te layer.

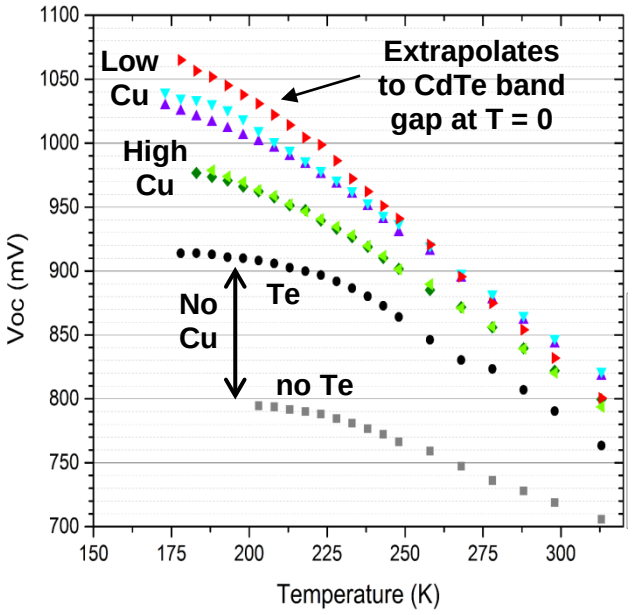

Figure 9. V_{oc} vs temperature for each of the cases in Fig. 8.

The likely explanation for the effectiveness of the Te layer can be seen in the band energies and Fermi levels of Fig. 10. CdTe has a relatively large (4.3 eV) electron affinity, which means that its valence maximum (VBM) of 5.8 eV is well below the vacuum level E_{VAC}. The nickel Fermi level shown (5.2 eV) is larger than that of other common metals and still well above the CdTe VBM. Hence, for the Fermi levels of CdTe and Ni to be equal, the CdTe bands are bent downwards, which produces a significant barrier for hole transport and a conduction band near the back that pushes electrons in the forward direction, the opposite direction to that of the photocurrent.

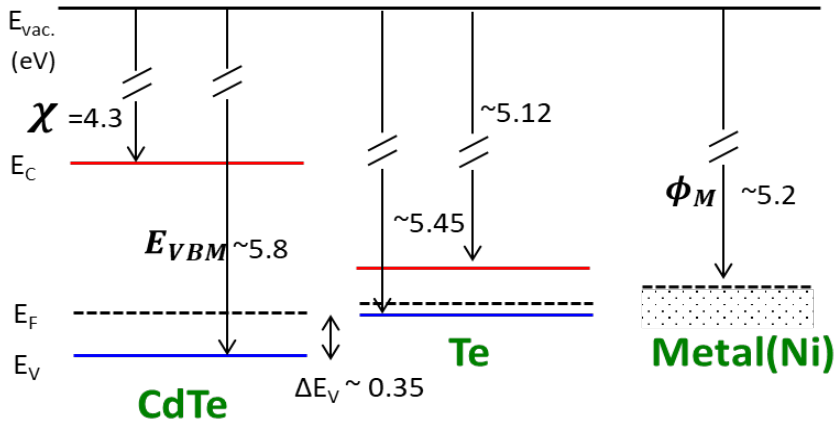

Figure 10. Relationship of CdTe and Te bands to the Fermi level of Ni

The band bending of CdTe when it directly contacts a metal such as the Ni above is pictured in Fig. 11(a), which shows that the holes are partially blocked from entering the metal and the electrons near the back will exit into the metal in the direction opposite to the cell's photocurrent. The hole barrier would be 0.6 eV if the CdTe Fermi level were at the VBM, but it is smaller because the typical CdTe carrier concentration is relatively small. It would, however, be somewhat larger for more heavily doped CdTe.

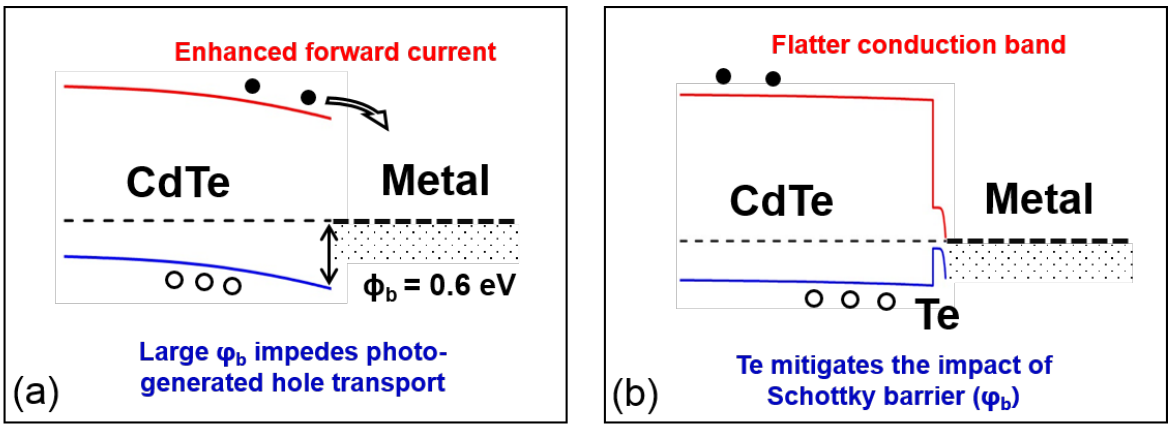

Figure 11. Band bending in CdTe with a metal contact (a) and Te layer (b).

The Fermi level of Te with its measured hole density is intermediate between that of CdTe and the metal. The result in Fig. 11(b) is less band bending in the CdTe and a

flatter band for electrons, but also a second hole barrier between the Te and the metal. The two smaller barriers, whose sum is the original 0.6-eV barrier, have less effect on the holes than a single larger one. Fig. 10(b) also shows why the thickness of the Te layer matters. If the Te is too thin, it cannot support a sufficient barrier, and the band diagram reverts towards that in 10(a).

Bilayer CdSeTe/CdTe Cells. In Year 2 of the project, the baseline cells transitioned from CdTe-only absorbers to thin CdSeTe/CdTe bilayers as shown in Fig. 1. This transition was motivated by success with this type of configuration at First Solar, but also by a band structure that argues for greater current collection with a lower-gap front layer and a step in the conduction band that moves the forward-current turn-on to a higher voltage relative to the band gap. It also turns out that CdSeTe tends to be a higher quality material than pure CdTe. The incorporation of CdSeTe for standard-thickness cells has been successful at several labs [19,20] and was used in this project for the thinner ones. This work also was done primarily by Alexandra Bothwell and Jennifer Drayton, but with considerable assistance from Pascal Jundt. Many of the results are published in Ref. [21].

Figure 12 compares the band structure of cells with a CdTe absorber to that with the additional CdSeTe/CdTe bilayer. In both cases, the total absorber thickness is 1.5 µm, and there was the MgZnO buffer at the front and the Te layer at the back as discussed above. The lower CdSeTe band gap allows more current generation in any case, but there is an additional important point concerning voltage. The two diagrams are shown for an applied forward bias of 1 V, which is the voltage region where the bands change from positive slope where the electric field assists photocollection to a flat or slightly negative slope where one would expect total current near zero. The key point is that the small step in the conduction band between CdSeTe and CdTe allows a similar front-to-back voltage difference as without the CdSeTe layer.

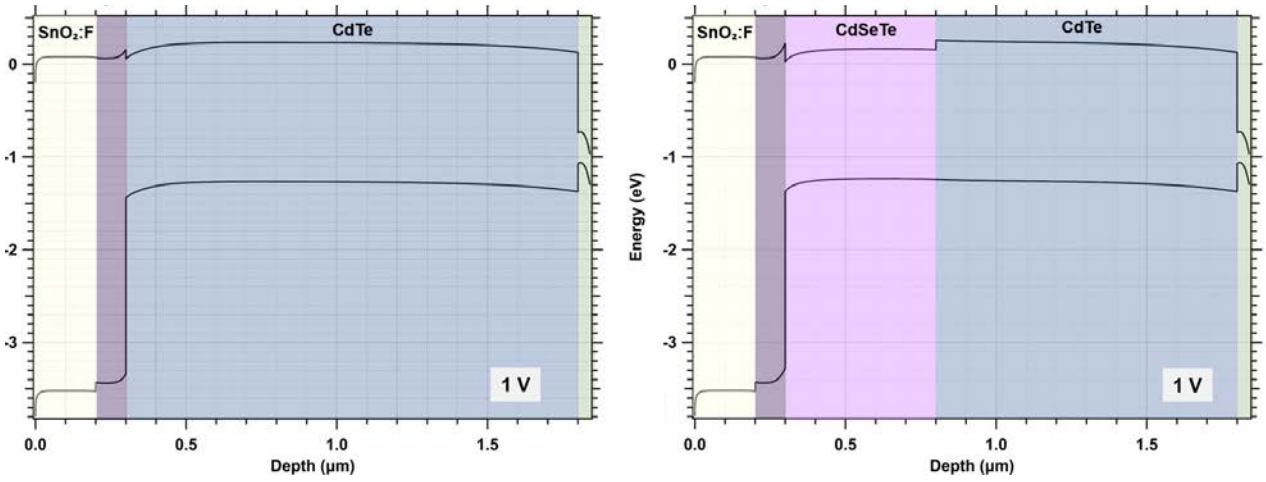

Figure 12. Band diagrams comparing CdTe and CdSeTe absorbers at a forward bias slightly higher than expected V_{OC}.

Physically the thin bilayer cells have had the desired elemental structure, which is shown in Fig. 13. The cross-section micrograph looks quite similar to Fig. 2 with the CdTe-only absorber. It also has grains extending across the cell, conformal Te and MgZnO layers top and bottom, and roughness the order of 0.1 µm. In this case though, one can clearly see the two absorber layers.

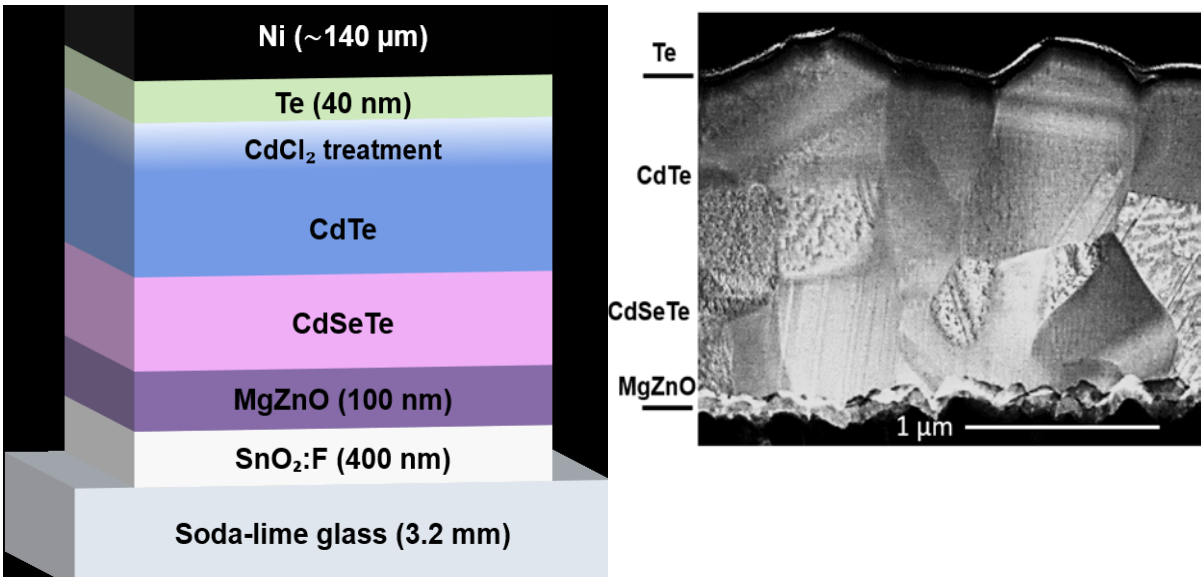

Figure 13. CdSeTe bilayer structure and corresponding STEM cross section.

The structure of the bilayer cells can also be clearly seen with their SIMS (secondary-ion mass spectrometry) profiles in Fig. 14, where the Se in the CdSeTe layer replaces approximately 10% of the Te and there is a small amount of Cl throughout from the passivation process. There is some broadening of the elemental transitions seen due to

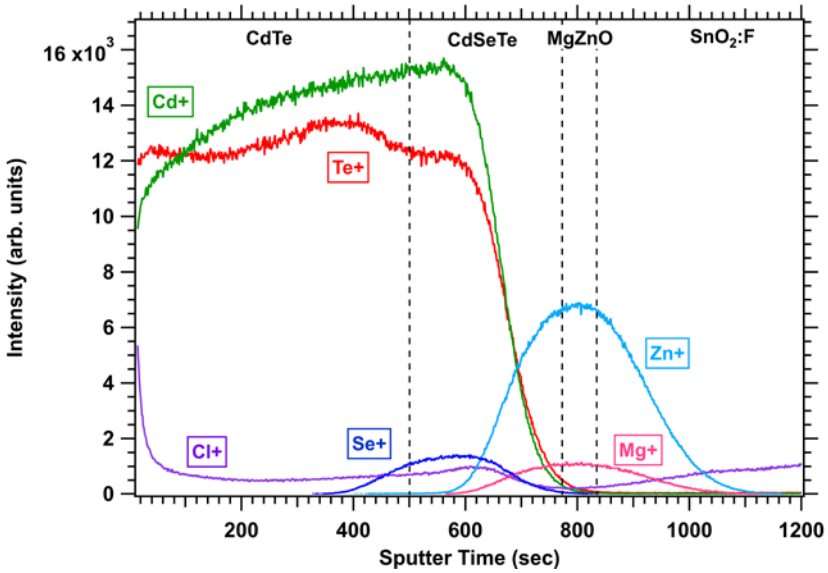

Figure 14. SIMS profile though a typical bilayer cell.

the roughness of the layers and interdiffusion during the SIMS sputtering process. The MgZnO layer, for example, is broadened by about 100 nm in either direction.

A comparison of current-voltage and quantum-efficiency curves from thin cells with and without the CdSeTe layer is given in Fig. 15. As expected the current increased by about 1.5 mA/cm^2 when the lower band-gap CdSeTe was included, as is clear in the QE curves at the right. The voltage was smaller, but by less than the band-gap difference, which means that the voltage deficit compared to the ideal was reduced. The fill-factor was slightly higher, and the net result was a 1% increase in absolute efficiency.

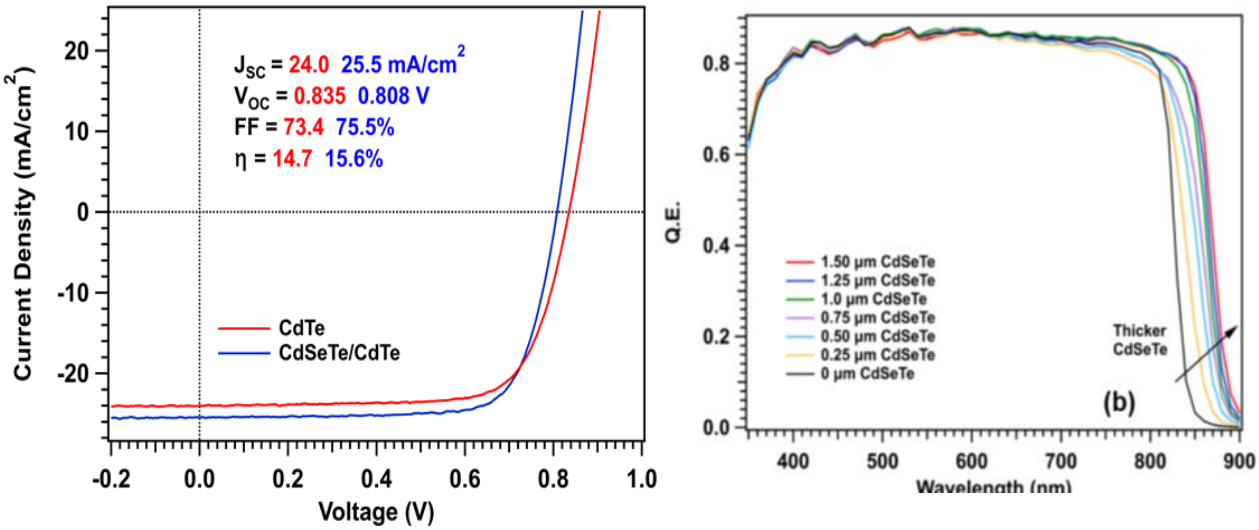

Figure 15. J-V and QE curves for CdTe-only and CdTeSe/CdTe cells.

The QE for the 1.5-μm CdTe cell in Fig. 16(a) is similar to that shown in Fig. 4, while Fig. 16(b) shows that a large majority of the QE (darker colored region) for the bilayer cell comes from the CdSeTe layer. Hence, since the absorption spectrum for photons

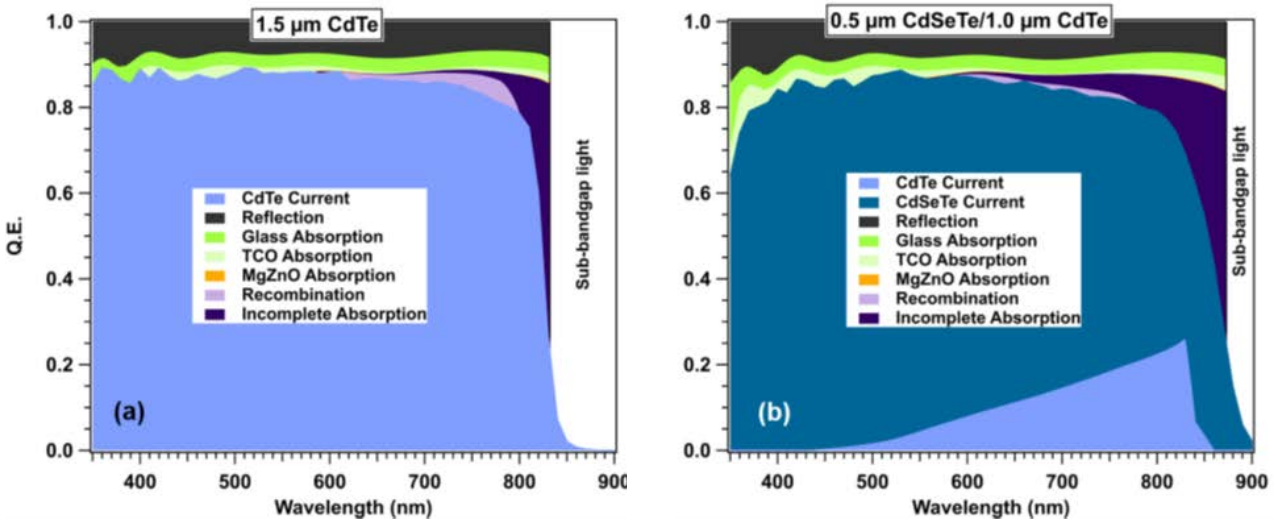

Figure 16. QE and individual photon losses in cells with and without the CdSeTe layer.

extends to longer-wavelengths photons, roughly 880 nm vs 840 in this case, for the smaller band-gap CdSeTe. In other information from Fig. 16, the individual photon losses from reflection and absorption in the layers before the absorber are fairly similar for the two cases. However, the roll-off near the bandgap is less sharp, because the transition between the two layers is not abrupt.

The optimal thickness of the CdSeTe was also investigated in detail. Fig. 16(b) shows that 0.5 µm is thick enough to absorb most of the light, and in practice it was found that the optimal thickness range is approximately 0.5 to 0.7 µm and that there is a significant fall-off in performance above 1 µm. Below 0.5 µm, less of the longer wavelength light is absorbed by the CdSeTe, and the variations in its thickness are proportionally larger.

A comparison of the fill factor-losses for the two cells in Fig. 16 is given in Fig. 17. The maximum fill factor for a CdTe absorber is just under 90%, and for the smaller band-gap CdSeTe, it is only slightly less. Because the cell voltage is less than its theoretical maximum, the fill-factor is also reduced, but only by a relatively small amount, which is shown in green for the two cases.

The additional breakdown of fill-factor losses was done using the analysis process described in Ref. [22]. The three parameters from the solar-cell diode equation:

$$J = J_0 \exp[(V - JR_S)/AkT] + GV - J_L$$

that are found in this analysis are the diode quality factor A, the series resistance R_S, and the leakage conductance G of the cell. The cell's photocurrent is given by J_L.

The losses from conductance (dark blue in Fig. 17) and series resistance (mid blue) are as expected fairly similar for the two cells. The diode quality factor, however, has been smaller when the CdSeTe alloy is used, and that is reflected in the smaller fill-factor loss in light blue. The narrow magenta region in the figure is simply the loss not accounted for.

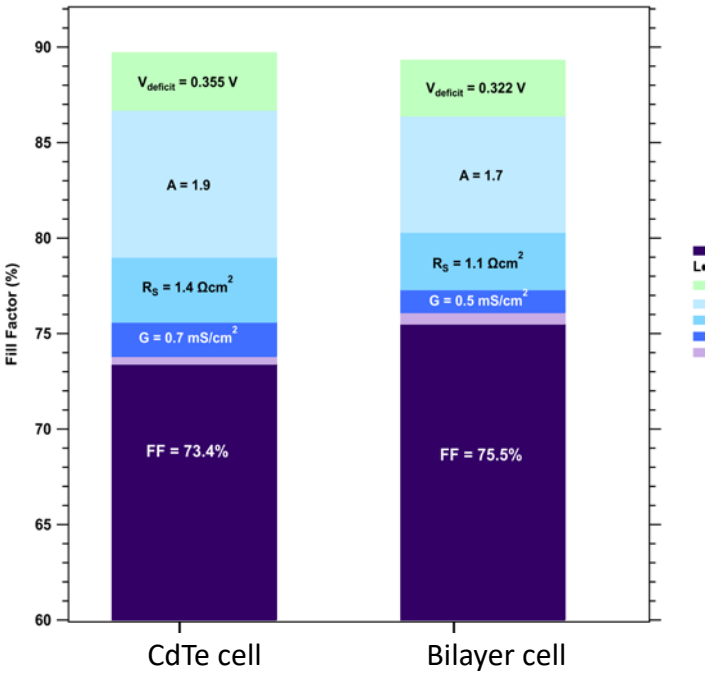

Figure 17. Individual fill-factor losses.

The larger fill-factor with the bilayer absorber suggests that the material quality of the CdSeTe layer is quite good, and additional evidence from luminescence lends strong support. Three different comparisons are shown in Fig 18. The spectral PL curves in Fig. 18(a), measured from the glass side of the cell, are centered as before near the band gap of the first absorber, and they show a very large difference in intensity between the CdTe cell and cells with CdSeTe of increasing thickness. This difference is more than a factor of ten.

Similarly, the time-resolved PL decays in Fig. 18(b), also measured from the front side, are very different between the two types of cell. The CdSeTe showed a much longer decay time which should correspond to its electron-hole recombination lifetime. The electroluminescence (EL) images in Fig. 18(c), formed by running equal currents through the two cells, is clearly brighter with the bilayer cell. This difference relates directly to the cells with the Se alloy having the smaller voltage deficit [23].

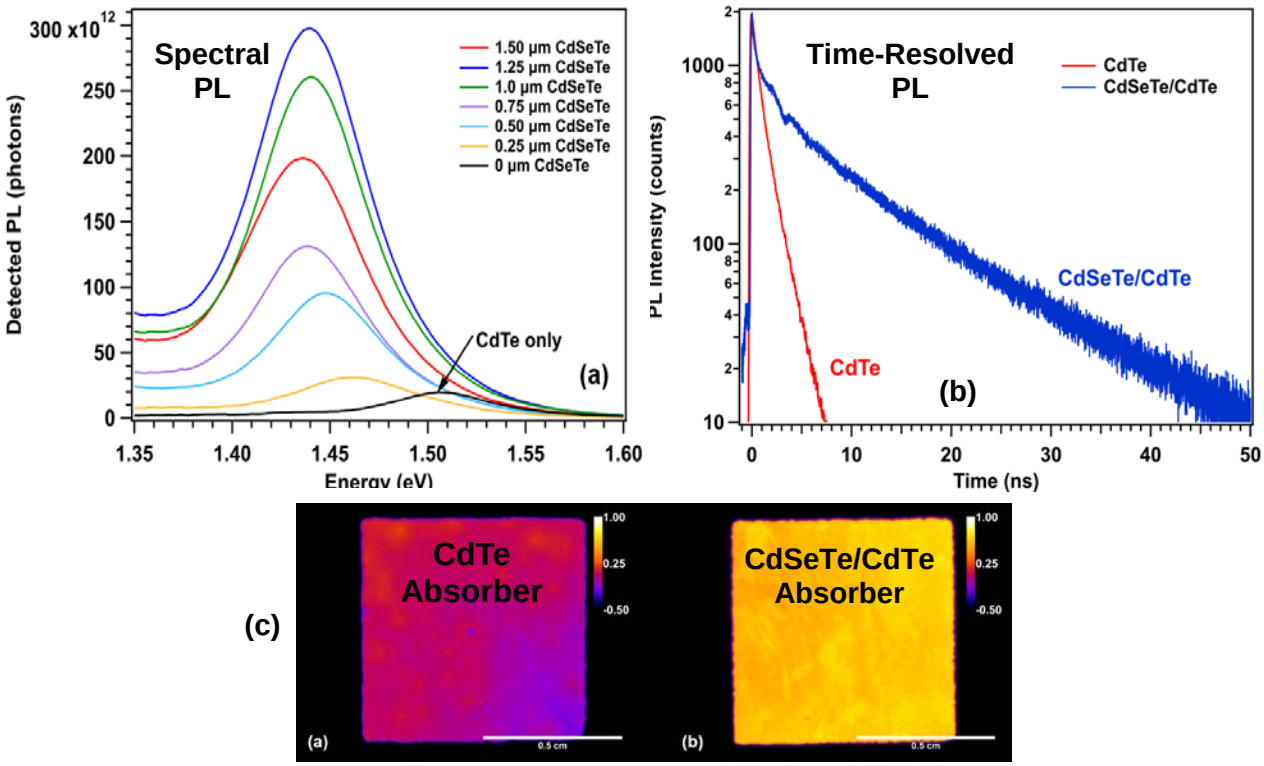

Figure 18. Cell quality comparison seen in PL spectra (a), time-resolved PL decays (b), and EL images (c).

Taken together with results from elsewhere, the work on cells with the CdSeTe/CdTe bilayer, provides convincing evidence that the transition to this structure was a good choice. There did need to be adjustments in the deposition temperatures and in the passivation process, but not large ones. Going forward, the introduction of a CdSeTe alloy layer into the absorber will also give flexibility in the design of cells with different carrier densities in different layers.

CdMgTe Layer for Electron Reflection. The Te layer described earlier was successful in mitigating the hole barrier at the back of the CdTe absorber, but it does not reflect electrons away from the back. An additional layer of CdMgTe with its conduction band extended upwards to reflect electrons was therefore added to the cell structure. This work, which began in Year 3 and extended into Year 4, built on the electron-reflection concept described in Ref. [24] and earlier work at Colorado State [25-26]. It also was primarily carried out by Alexandra Bothwell and Jennifer Drayton.

The concept of electron reflection from the back of a cell, sometimes referred to as a back-surface field, is illustrated in the Fig. 19 band diagrams. Figure 19(a) and (b) without the CdMgTe electron-reflection layer show the CdSeTe/CdTe cell as discussed previously. At zero and small biases (a), the slope of the bands gives an electric field that pushes electrons to the left and holes to the right, the directions for PV power generation, whereas at higher voltages (b), the slopes flatten and then reverse. The Te layer delays the reversal, but still allows electrons to escape from the back.

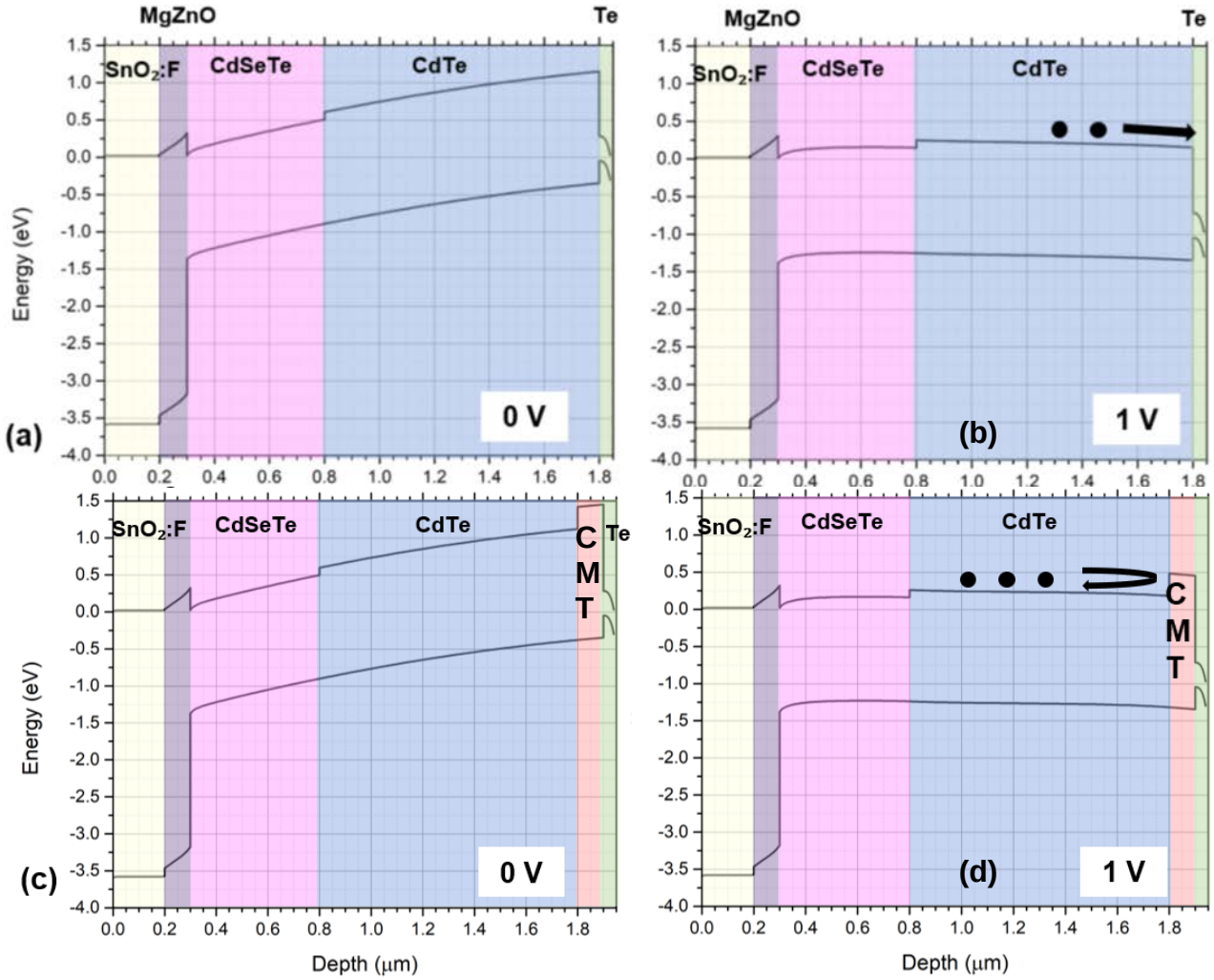

Figure 19. Band diagrams of cells at 0 and 1-V forward bias with and without a CdMgTe (CMT) electron-reflector layer.

The CdMgTe layer in Fig. 19(c) and (d) is designed to reflect the electrons away from the back contact of the cell and allow a higher voltage before the current direction is reversed. As shown there is a 0.2-V step in the conduction band and none in the valence band, which should be near-optimal conditions for electron reflection to be effective. There are, however, a number of other conditions for significant voltage enhancement including the passivation conditions of the rear interfaces, the carrier concentration of the CdMgTe layer, and its actual valence-band maximum.

The choice of CdMgTe for the electron-reflection layer was based on the tie line between CdTe and MgTe as seen in Fig. 20 where the position of the CdMgTe, abbreviated CMT, which was used in the cell structure, is highlighted. The lattice constant of MgTe is very close to that of CdTe, so that an alloy of the two will have a lattice constant quite close to that of CdTe, and hence one would expect a low defect density at the interface between them. Equally important, the band gap of MgTe is quite a bit higher than that of CdTe, and consequently, it does not take a large amount of Mg (15% was used) to produce an alloy with band gap 0.2-0.3 eV above that of CdTe

There are several other potential back-contact layers suggested by Fig 20. The other one commonly used is CdZnTe. Based on the arguments above, it would be a less attractive choice, but there are other reasons, such as its valence-band offset and the ability to dope it, that make it also a good candidate.

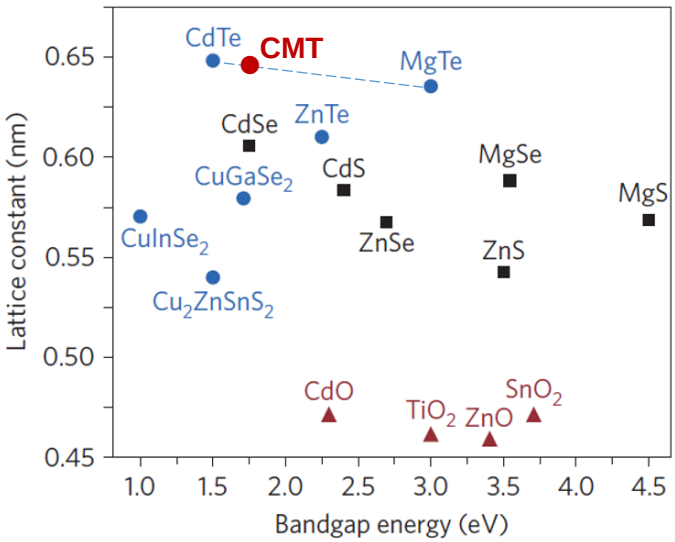

Figure 20. Relationship of CdTe lattice constant and band gap to those of similar materials.

The position of the valence band in Fig.19, as mentioned above, is important for the effectiveness of the CdMgTe layer, though it is not an easy quantity to measure with good accuracy. The traditional Kraut method [27] was applied to the layers being used in the project. It requires three structures as shown in Fig. 21 where x-ray photoelectron spectroscopy (XPS) can be referenced to core levels of CdMgTe and CdTe with the left and middle structures. The core-level difference can then be determined with the right-hand structure where the CdMgTe layer is thin enough that XPS signals from both it and the CdTe below can be measured.

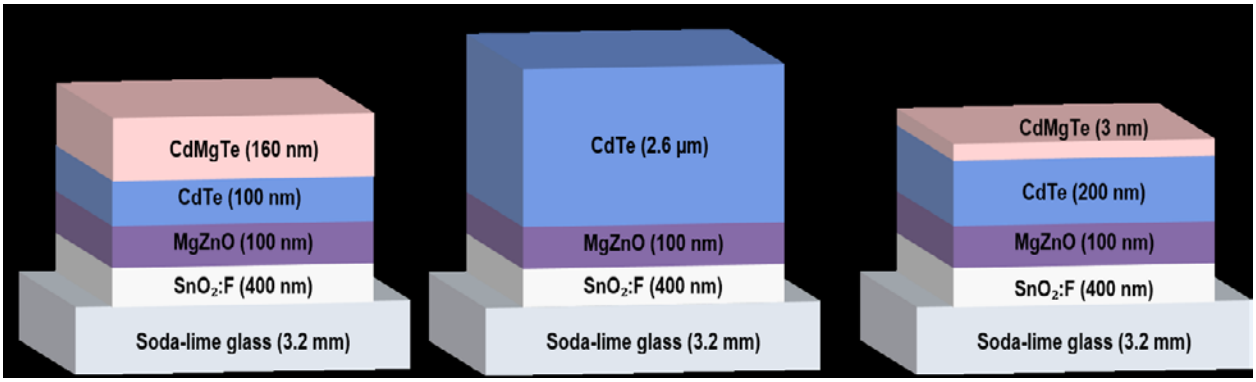

Figure 21. Structures terminating with CdMgTe, CdTe, and very thin CdMgTe covering CdTe, which were used for XPS determination of valence-band offset.

The result from the XPS measurements with the Fig. 21 structures was a valence-band offset which is 50-100 meV lower in the CdMgTe layer than in the CdTe. This is in the less-desired direction and would indicate that the voltage gain from the electron reflection would be less than a higher valence band for CdMgTe than for CdTe. A more accurate measurement of the offset should be possible with ultraviolet photoelectron spectroscopy (UPS), which was not available during the project period.

Earlier work at Colorado State had used close-space-sublimation deposition for both the CdTe and the CdMgTe layers [25,26]. However, the temperature required for CSS deposition drives off a part of the Cl used for grain-boundary passivation. Consequently, the CdMgTe layer is now being rf-sputter deposited at a lower temperature. The substrate temperature for the sputter deposition was found to be best set to between 150 and 200°C. Room-temperature (25°C) sputter deposition produced layers with less sharp x-ray peaks, which led to somewhat poorer cells. In the other direction, temperatures above 200°C appeared to also drive some of the Cl out of the CdTe and reduce the effectiveness of the passivation.

The current-voltage comparisons for the two types of CdMgTe deposition and the two temperatures used for the sputter deposition are shown in Fig. 22 (left). The difference between the 25°C (yellow) and 150°C (red) sputter-deposition temperatures is not large, but the higher temperature consistently produced cells with higher fill-factors, and both have out-performed the cells with CSS CdMgTe (purple). Capacitance-voltage curves (not shown) from cells with the two sputter temperatures were well-behaved, they were similar to each other, and they indicated a hole concentration in the 10^{14} cm^{-3} range over a large fraction of the CdTe.

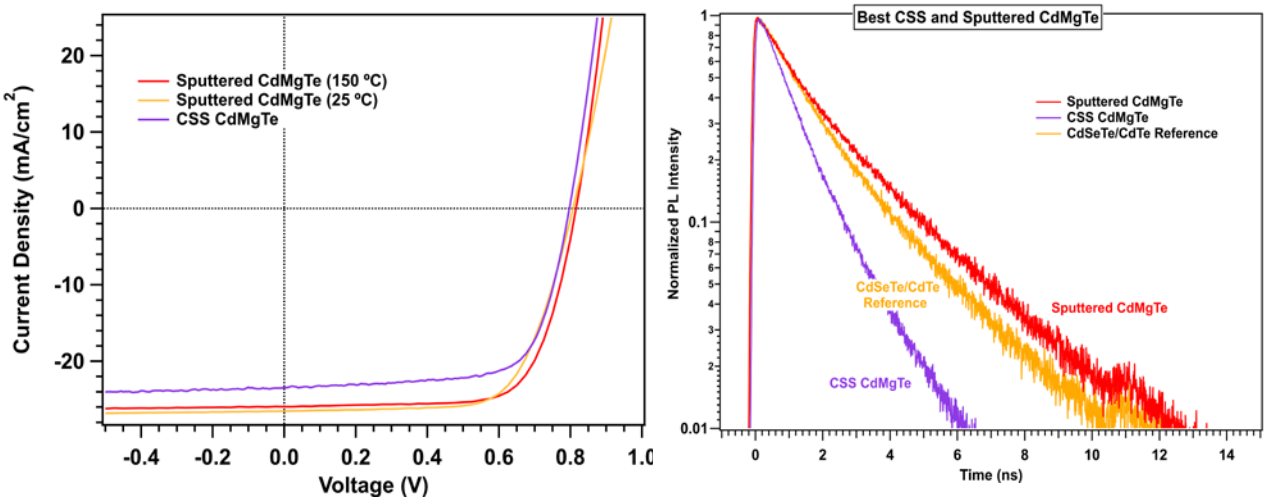

Figure 22. Current-voltage comparisons of cells with CdMgTe deposited by CSS and by sputtering at two temperatures (left) and TRPL comparison (right).

The difference between the two deposition techniques was significant in TRPL decay (Fig. 22 right) as well as in the resulting cell performance. The cell with CSS CdMgTe had the shortest decay time, while the sputtered CdMgTe had a decay time slightly

larger than a reference cell without CdMgTe, which implied that its interface recombination was less.

One question for development of the optimal CdMgTe layer is at what point in the deposition sequence does Cu-doping produce the best cells, and it was found earlier that it should be done after the CdMgTe is in place. An additional question is whether it should be done before or after the Te layer used for hole selectivity. The current-voltage comparison (Fig. 23, left) tells us that Cu-doping following the Te (Te/Cu shown in red), which is the cell order in Fig. 1, is preferred. The opposite order with copper first (Cu/Te in green) has a smaller fill-factor, and again the curve for a cell without CdMgTe (yellow) is included for comparison. The TRPL comparison in the right panel reinforces the point. The red Te/Cu decay is much slower than that of the green Cu/Te decay. In this case also, TRPL from a cell without CdMgTe is shown for reference.

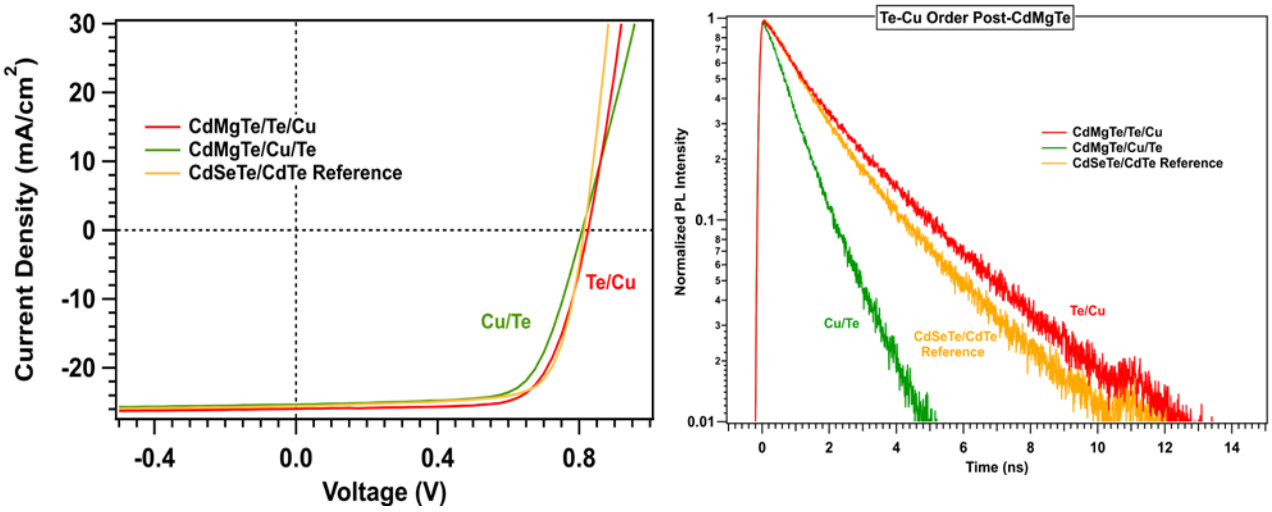

Figure 23. Current-voltage and TRPL comparison of Te/Cu deposition order.

Some insight on why the Te/Cu order is preferred can be seen in the SIMS profiles of Fig. 24. Magnesium on the left is present in the CdMgTe layer in similar amounts with

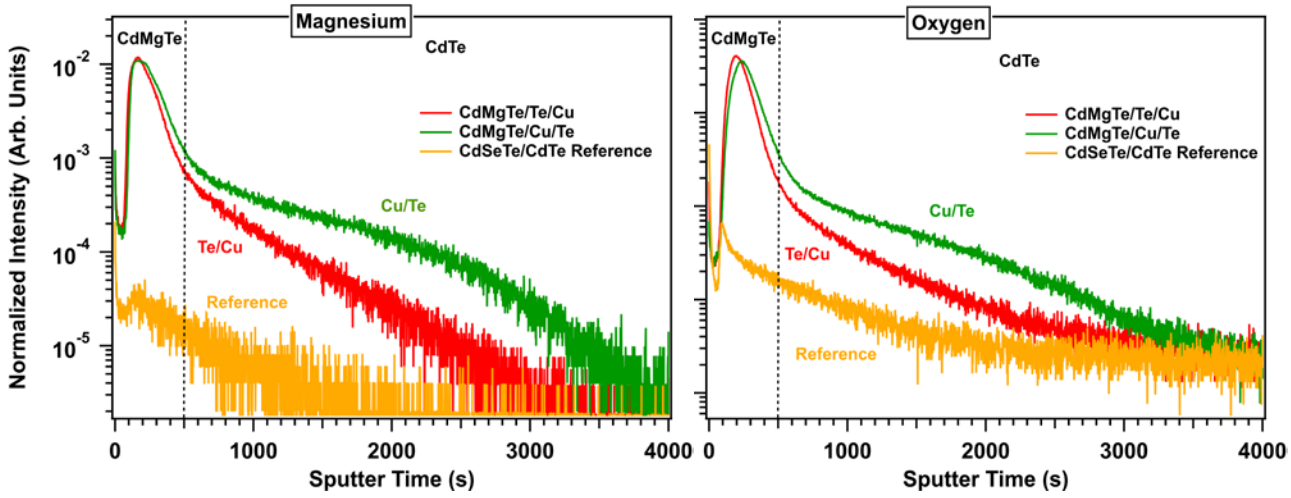

Figure 24. SIMS comparison of Te/Cu deposition order.

either order of Cu and Te, and it is only present in trace amounts in the reference sample without CdMgTe. However, more Mg and more oxygen on the right diffuse into the CdTe absorber when the Cu-doping is done first (green curves in both cases). This suggests that having the Te layer in place before the higher-temperature Cu-process provides a more effective barrier to oxidation within the CdTe absorber.

Two other steps in completing cells with the CdMgTe layer were investigated, but proved to be ineffective. In both cases the concern was oxidation in the Mg-containing layer. One step was an HCl etch following the CdMgTe deposition to remove any oxide. The HCl concentration needed to be weak to avoid damage, and when it was, the effect on the cell was neutral. The other step tried was a CdTe capping layer following the CdMgTe, again to prevent oxidation. In this case, cell performance was not as good, and the capping layer was also abandoned.

Figure 25 compares current-voltage curves that are calculated, but based on several cells with and without the CdMgTe electron-reflection layer, and with both thin bilayers and thicker ones. The cells these curves are based on had CdMgTe that was sputter deposited and their copper doping following their Te layer. The currents were slightly higher with the CdMgTe, and the fill-factors generally good. The thin-absorber cells without CdMgTe generally had the lowest voltage, followed by the thicker absorber without CdMgTe. Both the thin- and thick-absorber cells with the CdMgTe layer had the higher voltage, and these voltages were similar to each other.

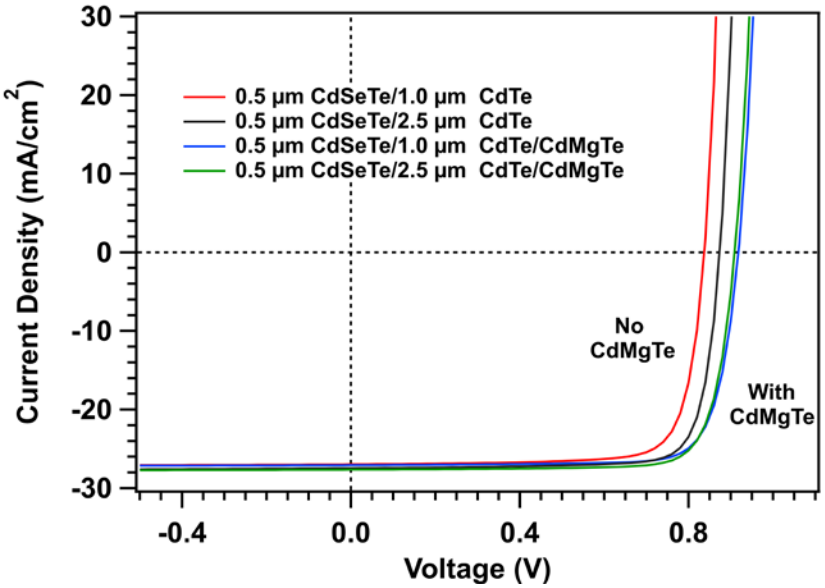

Figure 25. J-V comparison of thin-absorber cells, as well as thicker-absorber ones, with and without the CdMgTe electron-reflection layer.

The voltage differences in Fig. 25 and other comparisons were relatively small (~30 mV) compared to that which can be inferred from the band diagrams (>100 mV). The overall conclusion therefore is that electron reflection is shown to be helpful, but that the cell is not otherwise optimized, quite possibly because of the unfavorable CdMgTe valence-band offset.

Front Interface MgZnO Buffer. The use of an MgZnO emitter layer with CdTe instead of the traditional CdS layer has been quite successful at Colorado State [19]. Other groups, however, have informally reported difficulties with MgZnO, and our cells have sometimes seen changes in performance over time. The suspected problem has been a low electron density in MgZnO that varies according to processing details, is partially suppressed with exposure to short-wavelength light, and is more acute with higher hole-density absorbers. It was therefore decided during Year 4 of the project to investigate this issue in more detail both experimentally and with simulation. Ph.D. student Ramesh Pandey has done most of this work.

To show whether short-wavelength photons were critical, two cutoff filters with absorption spectra shown in Fig. 26(a) were used to remove or minimize photons with energy above the MgZnO band gap. With a CdS emitter (26b), the filters made no difference other than smaller total photocurrent. With the MgZnO emitter, however, there is a major kink in the J-V curves for either CdTe (26c) or the bilayer CdSeTe/CdTe (26d). There may also be a less noticeable distortion with the full solar spectrum.

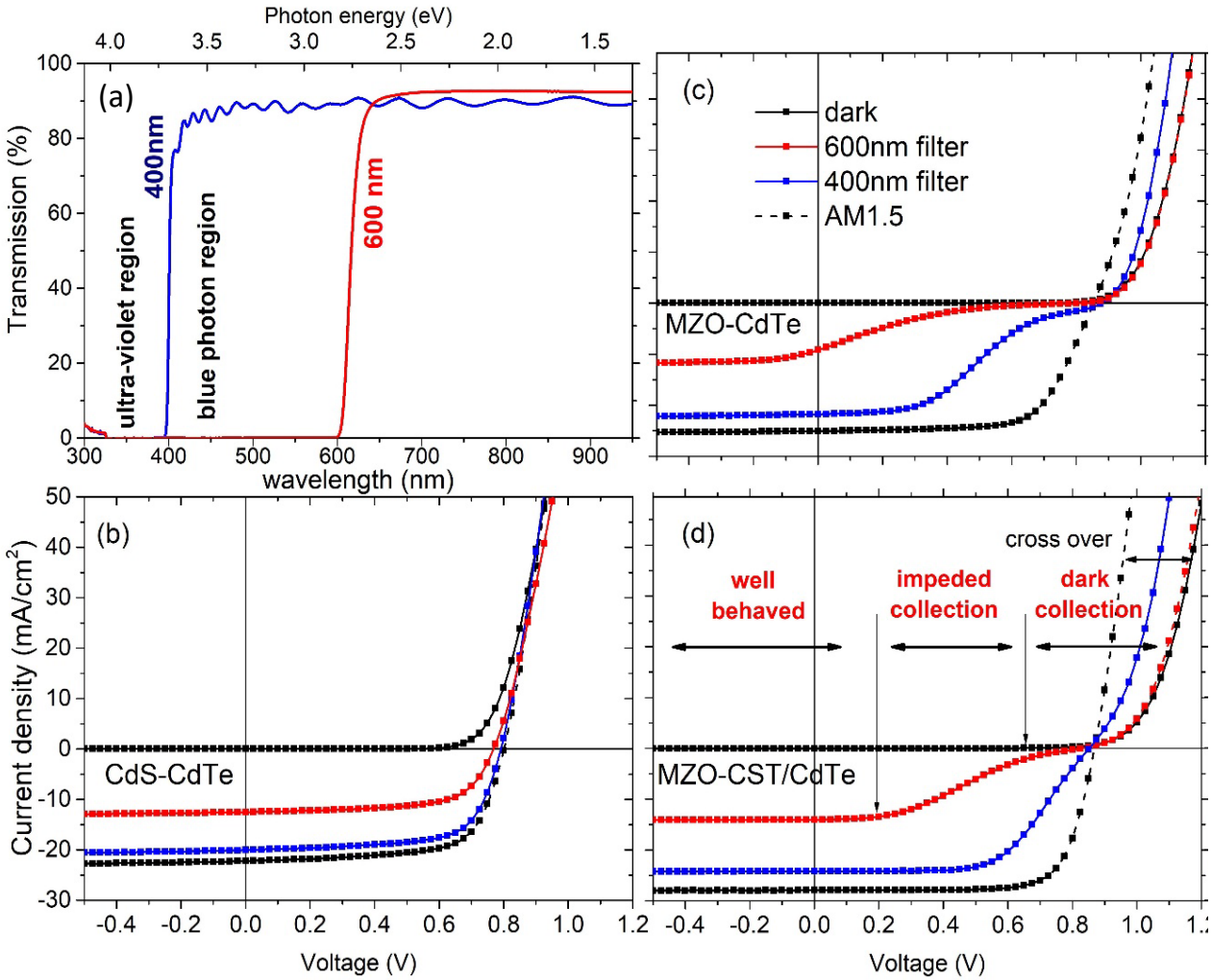

Figure 26. Effect of short-wavelength suppression with cutoff filters (a). J-V curves for three types of cells in (b), (c), and (d).

The J-V curves in Fig. 26 (c) and (d) are very similar to those in Ref. [28], and they are also very similar to those seen several years ago with CI(G)S cells that had various combinations of emitter materials and Ga-concentration [29,30]. In each of these cases, the absence of short-wavelength photons was responsible for the kink-like behavior, and when they were present, the kinks generally disappeared.

Figure 27 shows results from simulations based on the assumption that the short-wavelength photons create additional free electrons in the MgZnO by reducing compensation from deep acceptor levels. For four cases taken from Ref. [31], with two values each for bulk recombination and front-interface recombination S_{IF}, the calculated efficiency varies with the carrier density of both the absorber and the MgZnO emitter. The dashed line is particularly significant in that it delineates between the MgZnO density being larger or smaller than that of the absorber. The region below the dashed line has reduced efficiency because of the J-V kink shown in Fig. 26 above.

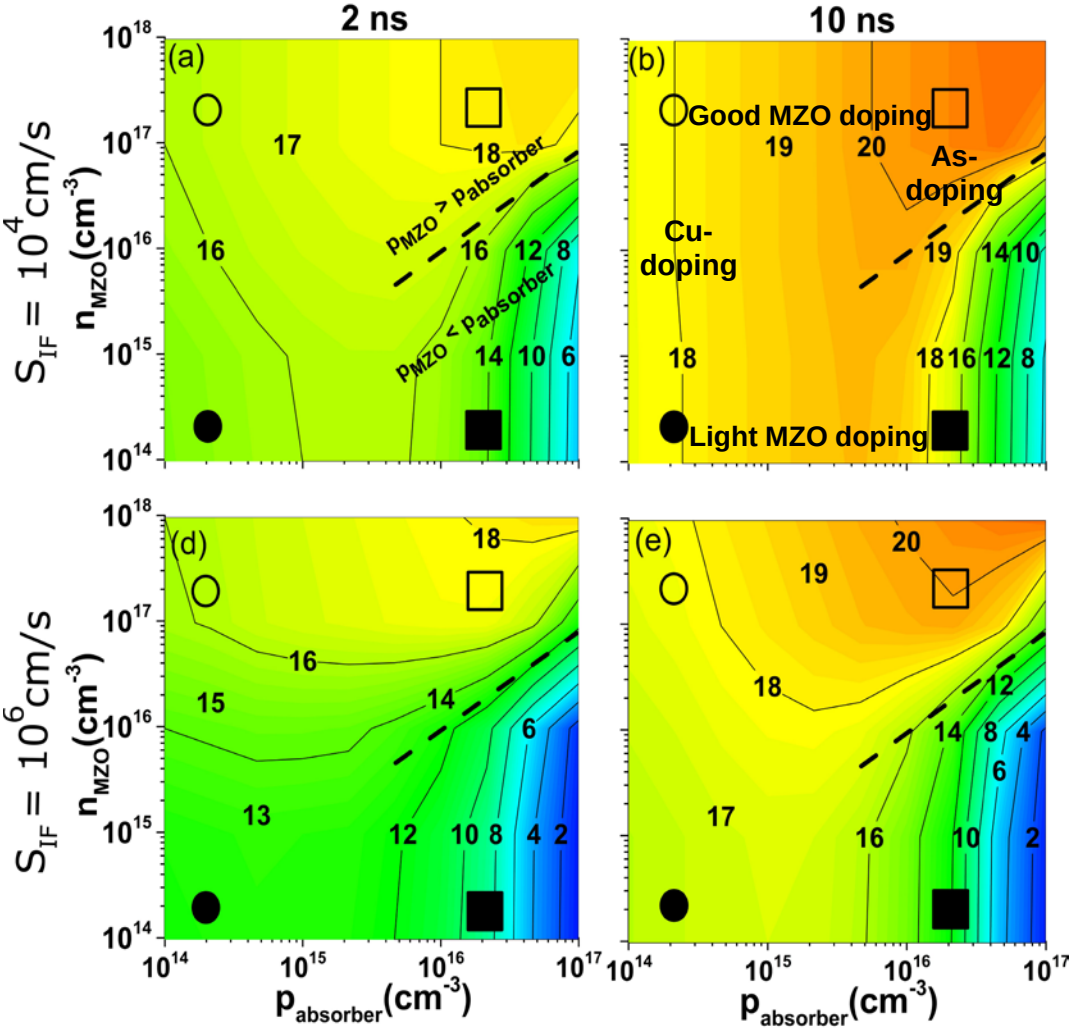

Figure 27. Calculations of efficiency as a function of MgZnO (MZO) and absorber carrier densities for two bulk lifetimes and front-interface recombination velocities.

Figure 28 makes the same point in for a still higher value of bulk recombination lifetime. The solid curves for high electron density in the MgZnO show a continuous increase in efficiency as the hole density in the absorber is increased that is eventually limited by the front interface recombination velocity. On the other hand, when the MgZnO density is low, the simulation shows a major drop off in efficiency for absorber densities above about 10^{15} cm^{-3}, which corresponds to the lower-right region in the of the Fig. 27 plots, and also to group-V absorber doping, which should otherwise be favorable.

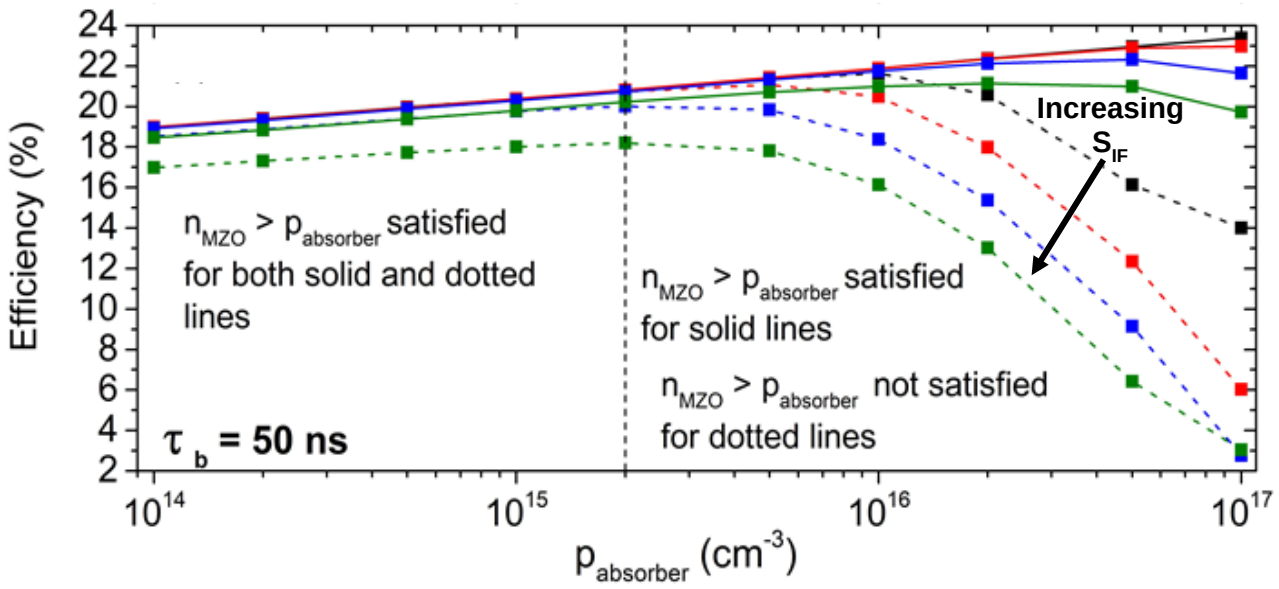

Figure 28. Calculated variation in cell efficiency as a function of absorber carrier density.

The reduction in compensation with the short-wavelength photons can mitigate the low MgZnO carrier density, as can a thinner layer or a reduction in the band offset [28], but the better choice is extrinsic n-type doping. Gallium was chosen as a good candidate for doing so, and a Ga-containing MgZnO (GMZO) sputter target was used to fabricate cells otherwise identical to those with J-V curves in Fig. 26. Current-voltage curves from a GMZO cell with filtered and unfiltered light, given in Fig. 29, show that the carrier density was sufficiently high without short-wavelength photons needed to enhance it.

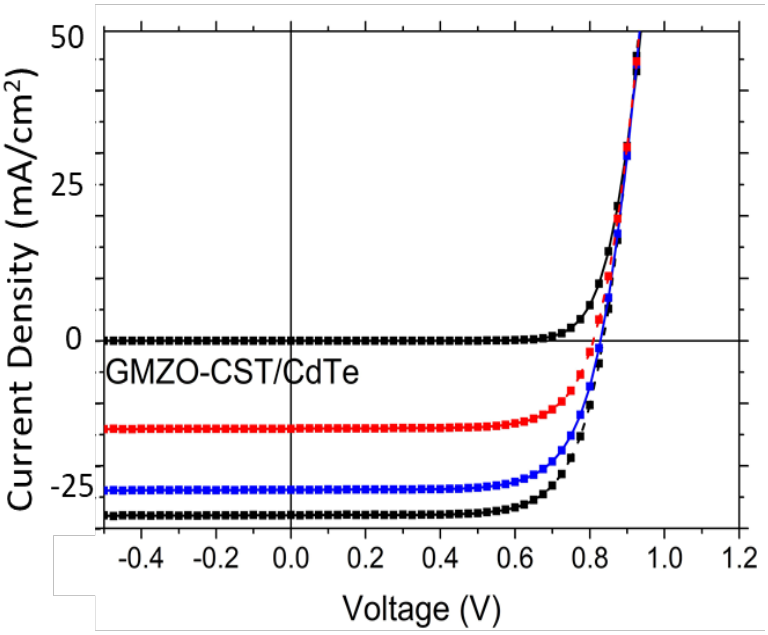

Figure 29. J-V with Ga-doped MZO.

There are a number of parameters involved in the best utilization of the MgZnO emitter layer, including the amount of Ga

or other material, the amount of Mg that determines the band offset, the thickness of the layer, and the carrier density of the absorber near the front interface. Additional work is clearly required, especially as we increase the absorber density from the 10^{14} cm^{-3} range where the MgZnO density is less important (left side of Figs. 26 and 27) to the higher CdTe densities needed to push efficiency to 25%.

Interpretation of Photoluminescence Data. The characterization and analysis tasks in the project took place throughout the four years and have generally been integrated into the previous sections. However, one category of characterization and analysis, photoluminescence (PL), has undergone considerable development over the course of the project and deserves extra attention. This area has included both spectral and time-resolved PL, and it has been carried out by PhD student Pascal Jundt and NREL staff member Darius Kuciauskas.

Early in the project, it became clear that a better spectral PL system was needed at Colorado State, and Pascal built the one shown in Fig. 30. It actually has two lasers of different wavelengths and appropriate filters to reject stray light. A substrate with several cells can be placed at the top of the light-tight box with a small external laser used for accurate positioning. Somewhat unique, however, a hinged set of probes could be used to apply a variable voltage across a cell during the measurements, which allowed a set of PL spectra over a range of cell bias as also shown in Fig. 31.

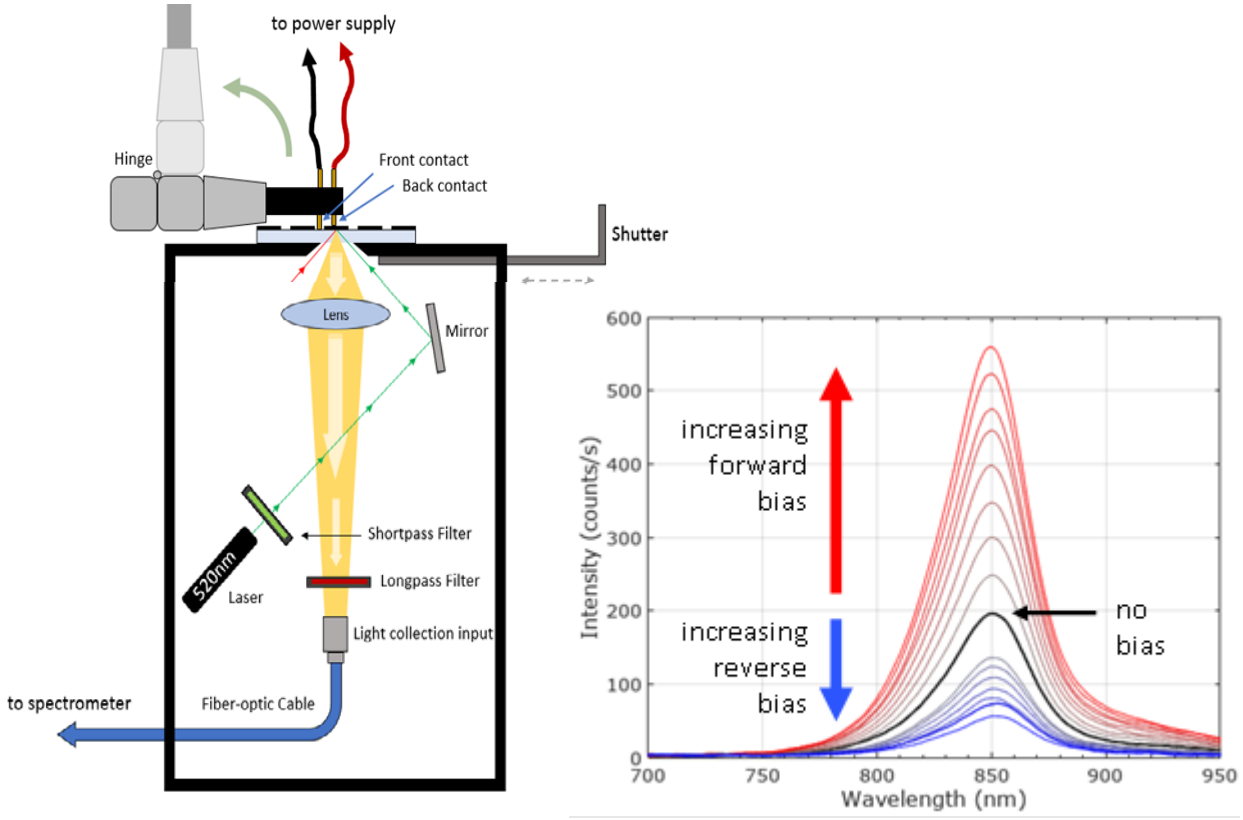

Figure 30. Spectral PL system with cell contacts to vary voltage (left) and example of large variation in PL intensity with voltage bias (right).

The PL peak in the Fig. 30 spectra has consistently been near 850 nm for cells with CdTe absorbers and somewhat higher for CdSeTe. The wide intensity range with bias across the cell is due to modification of the electric field in its primary diode. Clearly it is a large effect, and measurements made only at zero bias can be misleading. The intensity in sufficient forward bias to flatten the bands and eliminate the diode field is generally the most useful, though other considerations such as the intensity and penetration depth of the excitation laser are also important for comparing cells.

Time-resolved PL has been perhaps an even more valuable tool for comparing cell properties such as recombination lifetimes in cells with different structures and different processing conditions. There has been a long-term challenge, however, in separating the recombination parameters resulting from the front and back interfaces and the bulk material. This challenge is further complicated, as with spectral PL, by the separation of the photo-generated electrons and holes by the electric fields, and also by the role of carrier mobility in the diffusion of carriers away from the excitation location.

The key information driving TRPL is illustrated in Figure 31. Before an excitation pulse, there is a high density of electrons in a narrow region at the front of CdTe, a depletion region, and a relatively small hole density farther back, which is reduced further by the band bending near the rear contact. The absorption of the pulse falls exponentially with

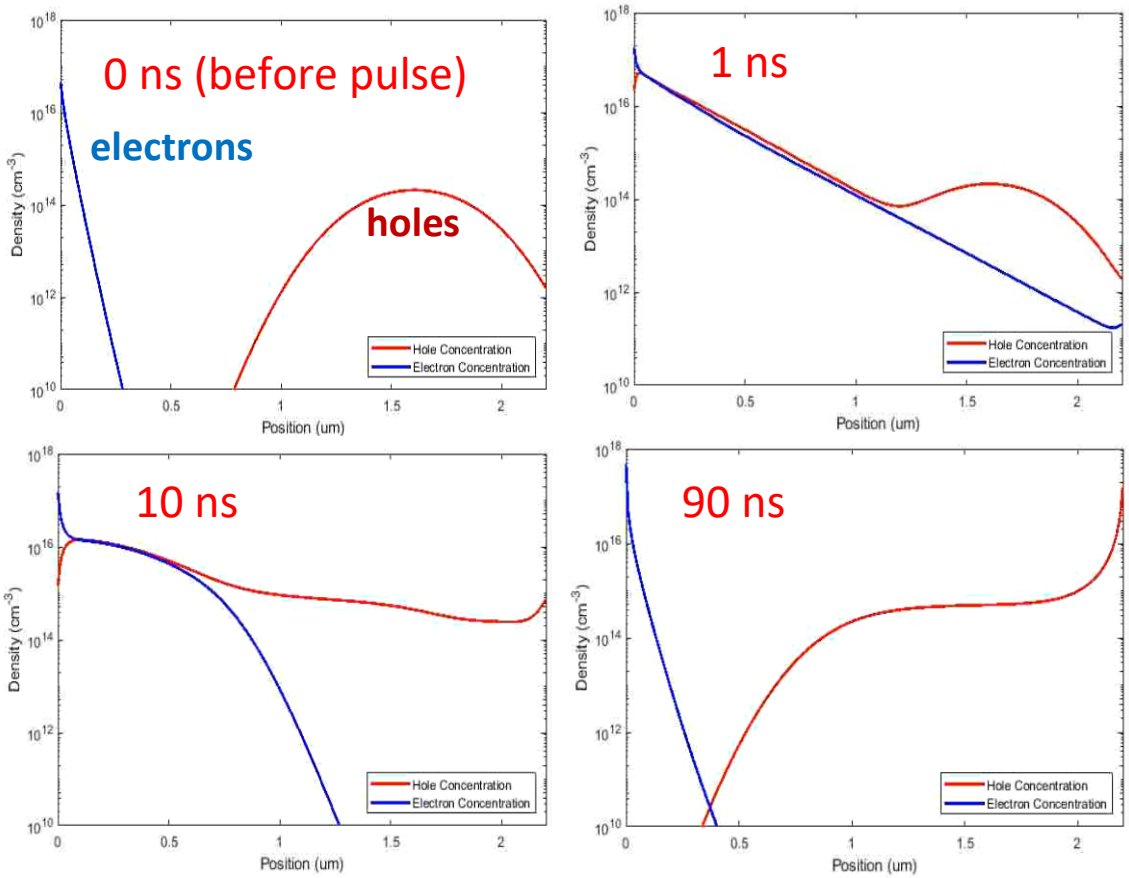

Figure 31. Simulated distribution of electrons and holes in a CdTe cell before a TRPL pulse and at key times afterwards.

its depth into the CdTe, and the emission at any time is the integrated electron-hole product times the local recombination rate. The relationship of the TRPL decay curves to specific materials and interface properties is complex, but the project did make considerable progress towards extracting useful information from the TRPL bias dependence.

Figure 32 shows a comparison of experimental TRPL data with simulations Pascal did using a software package developed at EMPA in Switzerland [32]. The experimental curves were measured at NREL with a typical Colorado State CdTe/CdSeTe-absorber cell, and the simulation incorporates the estimated device parameters from that cell. In this case, the illumination was from the front side and its penetration depth was approximately 0.2 µm. As with the spectral PL measurements, the dependence of the TRPL decay curves on the voltage bias across the cell is substantial, and here also the forward-bias decay where the bands are becoming flat gives the most credible results. The decay constant in the absence of a diode field can reasonably be assumed to be the lifetime of the bulk of the absorber.

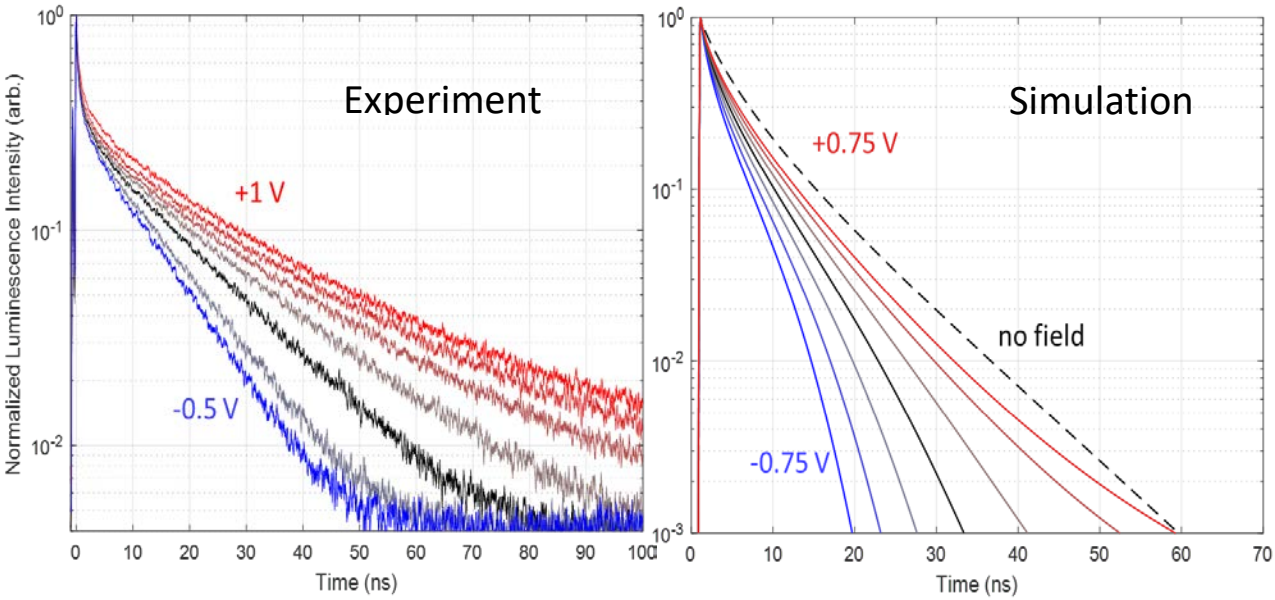

Figure 32. Experimental (left) and simulated (right) TRPL decay curves for different voltage bias across a cell. Black curves are for zero bias.

The spread in the TRPL curves with bias is also a function of the bulk CdTe lifetime. When the bulk lifetime is relatively small, the bias dependence is less of a factor, but with higher lifetime, the apparent bulk lifetime can be a factor of ten less than its actual value. As forward bias pushes the cell towards flat band, however, the difference becomes negligible. The elimination of the internal field makes the cell TRPL much like that of a field-free double heterojunction with small interfacial recombination, which should also give a reliable value of bulk lifetime. An obvious message is that one should measure TRPL decay with at least two biases, and reduce the cells' internal fields to the extent practical.

The deviation of the measured TRPL decay time, often denoted τ_2, from that of the true bulk lifetime was calculated and is shown in Fig. 33 for several values of voltage across the cell. The simulation, which again assumed parameters taken from experimental-cell data, showed that the measured decay time at zero voltage is about 30% too small for a bulk lifetime of 10 ns, and a factor of 3 too small if the bulk lifetime were 100 ns.

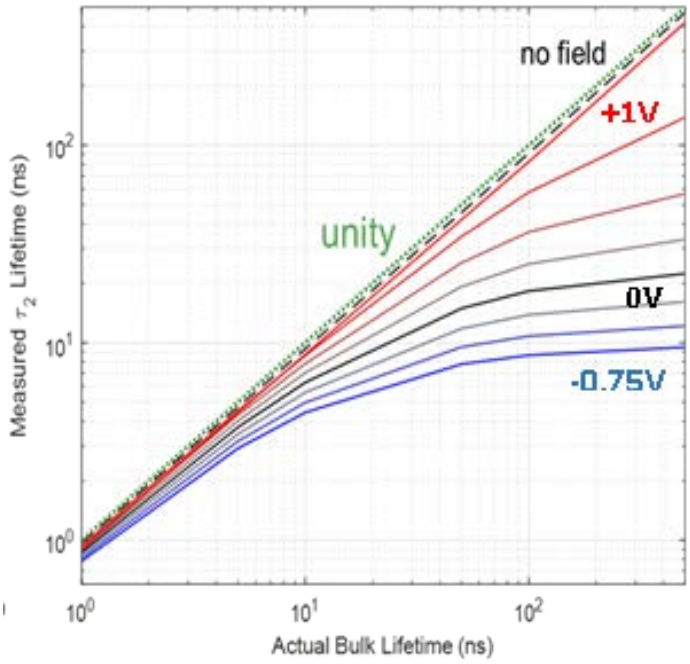

Figure 33. Deviation from true lifetime as a function of cell bias.

There is a wealth of additional information that can be gleaned from TRPL measurements. Probably most important is to design cell structures with transparent back contacts measurements near both the front and rear interfaces, and with 2-photon TRPL, measure an average decay time throughout the absorber. In addition to utilizing bias dependence and front-and-back excitation, additional TRPL measurement and simulation can greatly assist the determination of the key parameters limiting CdTe performance.

Conclusions

The central conclusion from the project is that all parts of the cell must work as designed both individually and in combination with each other. More specifically, the project found (1) that a thin absorber, 1-µm or less, is viable for CdTe cells, (2) that a Te layer at the back is effective in mitigating the band bending at a CdTe/metal interface, (3) that the bilayer CdSeTe/CdTe absorber has several advantages relative to CdTe by itself, (4) that CdMgTe can assist with electron reflection, but did not shown a major performance impact, (5) that a MgZnO emitter is effective, but needs to be more heavily doped, especially with higher carrier-concentration absorbers, and (6) that bias across a cell can substantially increase the value of time-resolved photoluminescence. Taken together and integrated with progress at other laboratories, the project has significantly helped to advance the understanding of several aspects of CdTe solar cells. With the exception of a clear advance in cell performance from electron reflection, the project met or exceeded its milestones.

Budget and Schedule. There were no changes in the project or spending schedule. The four years of the project corresponded to federal fiscal years, and expenditures were $240K in FY17, $221K in FY18, $254K in FY19, and $280K in FY20 for a total just under the $900K budgeted. The 10% University cost-share was kept consistently ahead of the federal funding and met the $100K commitment.

Path Forward

The path forward within the larger CdTe community for the further development of the CdTe technology, particularly results that have a direct impact on cell performance, can be divided into three primary areas: low-recombination at the front interfaces of the cell, an absorber configuration that includes a high hole concentration and a low bulk recombination, and back-contact layers that direct holes towards the contact and electrons away from it. At the same time, the research initiatives must continue to be consistent with industrial fabrication costs that are equal or less than those at present.

The major CdTe device projects at Colorado State in support of this path are currently:

(1) Back-contact interface engineering for higher-efficiency CdTe PV (DOE funded, Sites PI). This collaboration of five institutions led by CSU focuses on the CdTe back contact, believed to be the largest voltage limitation at present. The goal is to simultaneously have a highly passivated contact and a band structure that allows both hole transport and electron reflection.

(2) Doping CdTe and CdSeTe for higher efficiency (DOE funded, Sampath PI). The project goal is to utilize As-doping to increase the absorber carrier density and eliminate the use of copper. The emphases are on achieving a high fraction of As atoms located on substitutional sites and achieving an optimal design for the CdTe and CdSeTe-alloy layers.

Smaller continuing projects at Colorado State include:

(1) Interpretation of TRPL results (DOE funded, Sites PI). Completion of the project to utilize variations in cell bias and excitation location and intensity to extract the true recombination lifetimes of the cell absorber and front and back interfaces.

(2) Diagnosing and overcoming recombination in CdTe (DOE funded, Sampath PI). Subcontract from ASU to better passivate back surface of CdTe.

(3) Framework for CdTe voltage losses (NSF funded, Sites PI). Joint project to separate and quantify the CdTe voltage losses in First Solar and CSU cells.

(4) DFT calculations of CdTe interfacial defects (NSF funded, Sampath PI). Position and energy defect profiles based on fundamental semiconductor physics.

(5) Ga-doped MgZnO emitter layers (NSF funded, joint PI's). Completion of project to increase the carrier density of MgZnO with emphasis on As-doped absorbers.

Publications, Conference Presentations, and Degrees

Publications.

(1) Tao Song, Andrew Moore, and James R. Sites, "Te layer to reduce the CdTe back-contact barrier," IEEE J. Photovoltaics **8**, 293-298 (2018). doi:10.1109/JPHOTOV.2017.2768965

(2) Alexandra M. Bothwell, Jennifer A. Drayton, Pascal M. Jundt, and James R. Sites, "Characterization of thin CdTe solar cells with a CdSeTe front layer," MRS Advances **4**, 37 (2019). doi10,1137/adv/2019.332

(3) Alexandra Bothwell, Jennifer Drayton, and James Sites, "Performance analysis of 0.4 to 1.2 µm CdTe solar cells," IEEE Journal of Photovoltaics **10**, 259-265 (2020). doi10/1109/JPHOTOV.2019.2947556

(4) Alexandra Bothwell, Jennifer Drayton, Pascal Jundt, and James Sites, "Close-space-sublimation-deposited ultra-thin CdSeTe/CdTe solar cells for enhanced short-circuit current density and photoluminescence," Journal of Visualized Experiments (JoVE) **157** (2020). doi:10.3791/66937
(5) Ramesh Pandey, Tushar Shimpi, Amit Munshi, and James Sites, "Impact of carrier concentration and carrier lifetime on MgZnO/CdSeTe/CdTe solar cells," IEEE J. Photovoltaics, doi.10.1109/JPHOTO.2020.30117741, in press.

Conferences Presentations.

(1) Anna Wojtowicz, Alexandra Huss, Jennifer Drayton, and James Sites, "Effects of $CdCl_2$ passivation on thin CdTe solar cells fabricated by close-space sublimation," IEEE PVSC-44, Washington DC, June 2017.
(2) Tao Song and James Sites, "Role of tellurium buffer layer on CdTe solar cells' absorber/back-contact interface," IEEE PVSC-44, Washington DC, June 2017
(3) James Sites, Amit Munshi, Drew Swanson, Andrew Moore, Tao Song, and W.S. Sampath, "Enhancements to CdTe efficiency," Plenary talk at EU-PVSEC-34, Amsterdam, September 2017.
(4) Alexander M. Huss, Jennifer A. Drayton, and James R. Sites, "Front and back interface recombination of MZO/CdTe/Te solar cells," 7th World PV Science and Engineering Conference, Jun 2018.
(5) James Sites, Amit Munshi, Tal Song, Alexandra Huss, and W.S. Sampath, "Solar cells with ternary CdSeTe absorbers," 21st Intl. Conf. on Ternary and Multinary Compounds, Boulder, CO, September 2018.
(6) James Sites, Alexandra Huss, and Tao Song, "Increased efficiency with CdSeTe in front of CdTe," EU-PVSEC-35, Brussels, September 2018.
(7) James Sites, "Solar cells with bilayer CdSeTe/CdTe absorbers," 54th Conf. on Microelectronics, Devices, and Materials, Ljubljana, Slovenia, October 2018.
(8) Alexandra Bothwell, Jennifer Drayton, Pascal Jundt, and James Sites, "Characterization of thin CdTe solar cells with a CdSeTe layer in front," Spring MRS Meeting, Phoenix, AZ, April 2019.
(9) James Sites and Pascal Jundt, "Device structure of high-efficiency thin-film CdTe solar cells," 15th PV Science Applications, and Technology Conf., Warwick, UK, April 2019.
(10) Alexandra Bothwell, Jennifer Drayton, Pascal Jundt, and James Sites, "CdMgTe as an electron reflector for MgZnO/CdSeTe/CdTe solar cells," IEEE PVSC-46, Chicago, June 2019.
(11) Pascal Jundt, Darius Kuciauskas, and James Sites, "Field effect in CdSeTe/CdTe solar cells with biased spectroscopy," PVSC-46, Chicago, June 2019.
(12) D. Kuciauskas, J. Moseley, D. Albin, A. Munshi, A. Danielson, C. Reich, W. Sampath, A. Onno, Z. C. Holman, C. Lee, and D. Krasikov, "Origin of microsecond charge carrier lifetimes in polycrystalline CdTe solar cells," Invited presentation at Virtual Chalcogenide PV Conference, May, 2020
(13) Pascal Jundt, Darius Kuciauskas, and James Sites, "Simulating the effect of p-n junction fields on TRPL transients of CdSeTe/CdTe thin-film solar cells," IEEE PVSC-47, June, 2020.

(14) Alexandra Bothwell, Jenifer Drayton and James Sites, “Efficiency advances in thin CdSeTe solar cells with CdMgTe at the back”, IEEE PVCS-47, June 2020.
(15) James Sites, Cherry Award acceptance. Keynote talk at the June 2020 IEEE PV Specialists Conference.

Degrees Completed

(1) Tao Song, Ph.D., Spring 2017, employment at NREL
(2) Andrew Moore, Ph.D., Summer 2017, employment at Intel
(3) Anna Wojtowicz, M.S., Fall 2017, employment at MiaSolé
(4) Alexandra Bothwell, Ph.D., Fall 2020, continuing at Colorado State

Acknowledgements

Research Associate Jennifer Drayton and PhD students Alexandra (Huss) Bothwell and Pascal Jundt, as well as the PI, worked directly on the project throughout. Postdocs Tao Song and Andrew Moore, Darius Kusciauskas at NREL, Ph.D. student Ramesh Pandey, and M.S. student Anna Wojtowicz worked on the project for parts of the four years. In addition, co-PI W.S. Sampath contributed greatly through many discussions, Amit Munshi and Kevan Cameron through equipment maintenance and upgrades, and Michael Walker at the Colorado School of Mines with the SIMS measurements.

References

[1] N. Steyl, L. Trippel, C. Kotarba, and I Khan, “Improvements in CdTe module reliability and long-term degradation through advances in construction and device innovation,” Photovoltaics International **22,** 66-74 (2013).

[2] A. Rix, J.D.T. Steyl, M.J. Rudman, U. Terblanche, and J.L. van Niekerk, “First Solar’s CdTe module technology – performance, life cycle, health and safety assessment,” Center for Renewable and Sustainable Energy Studies (2015).

[3] M.J. Markiska and de Wild-Scholten, “Energy payback time and carbon footprint of commercial photovoltaic systems,” Solar Energy Materials and Solar Cells **119,** 296-305 (2013).

[4] First Solar 2019 Annual Report. https://investor.firstsolar.com/financials/annual-reports/default.aspx

[5] W.K. Metzger, S. Grover, D. Lu, E. Colegrove, J. Moseley, C.L. Perkins, X. Li, R. Mallick, W. Zhang, R. Malik, J. Kephart, C.S. Jiang, D. Kuciauskas, D.S. Albin, M.M. Al-Jassim, G. Xiong, and M. Gloeckler, “Exceeding 20% efficiency with in situ group V doping in polycrystalline CdTe solar cells,” Nat Energy **4,** 837-845 (2019).

[6] A.M. Bothwell, J.A. Drayton, P.M. Jundt, and J.R. Sites, “Close-space-sublimation-deposited ultra-thin CdSeTe/CdTe solar cells for enhanced short-circuit current density and photoluminescence,” Journal of Visualized Experiments (JoVE) **157** (2020).

[7] A.M. Bothwell, J.A. Drayton, and J.R. Sites, “Performance analysis of 0.4 to 1.2 µm CdTe solar cells,” IEEE Journal of Photovoltaics **10**, 259-265 (2020).

[8] A. Gupta, V. Parikh, and A.D. Compaan, “High efficiency ultra-thin sputtered CdTe solar cells,” Solar Energy Mat. Solar Cells **90**, 2263-2271 (2006).

[9] V. Plotnikov, X. Liu, N. Paudel, D. Kwon, K. Wieland, and A. Compaan, Thin-film CdTe cells: reducing the CdTe," Thin Solid Films **519**, 7134-7137 (2011).

[10] N. Paudel, K. Wieland, and A. Compaan, "Ultrathin CdS/CdTe solar cells by sputtering," Solar Energy Mater. Solar Cells **105**, 109-112 (2012).

[11] E. Jones, V. Barrioz, S. Irvine, and D. Lamb, "Towards ultra-thin CdTe solar cells using MOCVD," Thin Solid Films **517**, 2226-2230 (2009).

[12] B.E. McCandless and W.A. Buchanan, "High throughput processing of CdTe/CdS solar cells with thin absorber layers," Proc. 33rd IEEE Photovoltaics Specialists Conf. (2008).

[13] T. Song, A. Moore, and J.R. Sites, "Te layer to reduce the CdTe back-contact barrier," IEEE J. Photovoltaics **8**, 293-298 (2018).

[14] A. Moore, T. Song, and J.R Sites, "Improved CdTe solar-cell performance with an evaporated Te layer before the back contact," MRS Advances **2,** 3165-3171 (2017).

[15] H. Uda, S. Ikegami, and H. Sonomura, "Te-metal contact on evavaporated CdTe film for a CdS/CdTe solar cell." Solar Energy Mater. Solar Cells **35**, 293-298 (1994).

[16] T. Potlog, L. Ghimpu, and C. Antoniuc, "Comparitive study of CdS/CdTe cells fabricated with and without evaporated Te-layer," Thin Solid Films **515**, 5824-5827 (2007).

[17] R. Ochoa-Landin, R.O. Vigil-Galan, Y.V. Vorobiev, and R. Ramirez-Bon, "Chemically-deposited Te layers improving the parameters of back contacts for CdTe solar cells," Solar Energy **83**, 134-138 (2009).

[18] W. Xia et al, "Te/Cu bi-layer: a low-resistance back contact for thin film CdS/CeTe solar cells," Solar Energy Mater. Solar Cells **128**, 411-420 (2014).

[19] A.H. Munshi et al, "Polycrystalline CdSeTe/CdTe absorber cells with 28 mA/cm^2 short-circuit current," IEEE J. Photovoltaics 8, 310-314 (2017).

[20] T. Ablekim et al, "Thin-film solar cells with 19% efficiency by thermal evaporation of CdSe and CdTe," ACS Energy Letters 5, 892-896 (2020).

[21] A.M. Bothwell, J.A. Drayton, P.M. Jundt, and J.R. Sites, "Characterization of thin CdTe solar cells with a CdSeTe front layer," MRS Advances **4**, 37 (2019).

[22] S.S. Hegedus and W.N. Shafarman, "Thin-film solar cells: device measurements and analysis," Prog. Photovoltaics: Res. Appl.**12**, 155-176 (2004).

[23] M. Bokalič, J.M. Raguse, J.R. Sites, and M. Topič, "Analysis of electro-luminescence images in small-area circular CdTe solar cells," J. Appl. Phys. **114**, 123102 (2013).

[24] K.-J. Hsiao et al, "Electron reflector to enhance photovoltaic efficiency," Prog. Photovoltaics: Res. Appl. **20**, 486-489 (2012).

[25] P.S. Kobyakov et al, "Deposition and characterization of CdMgTe thin films grown by a novel co-sublimation method," J. Vac. Sci. Technol. **A32**, 021511 (2014).

[26] D.E. Swanson et al, “Incorporation of CdMgTe as an electron reflector for cadmium telluride photovoltaic cells,” MRS Online Proc. Library Archive, **1771**, 133-138 (2015).

[27] E.A. Kraut, R.W. Grant, J.R. Waldrop, and S.P. Kowalczyk, “Precise determination of the valence-band edge in x-ray photoemission spectra: application to measurement of semiconductor interface potentials,” Phys. Rev. Letters **44**, 1620-1623 (1980).

[28] D.-B. Li, et al, “Eliminating the S-kink to maximize performance ot MgZnO/CdTe solar cells,” ACS Appl. Energy. Mat

[29] I.L. Eisgruber, J.E. Granta, J.R. Sites, J. Hou, and J. Kessler, “Blue-photon modification of nonstandard diode barrier in $CuInSe_2$ solar cells,” Solar Energy Mater. Solar Cells **53**, 367-377 (1998).

[30] A.O. Pudov, A. Kanevce, H.A. AlThani, J.R. Sites, and F.S. Hasoon, “Secondary barriers in CdS-CIGS solar cells,” J. Appl. Phys. **97**, 064901 (2005).

[31] R. Pandey, T. Shimpi, A. Munshi, and J.R. Sites, ““Impact of carrier concentration and carrier lifetime on MgZnO/CdSeTe/CdTe solar cells,” IEEE J. Photovoltaics, in press.

[32] T.P. Weiss et al, “Bulk and surface recombination properties in thin-film semiconductors with different surface treatments from time-resolved photoluminescence measurements,” Sci. Rep. **9**, 5385 (2019).